POLITECNICO DI TORINO
1859 1906

M.Sc. Nanotechnologies for ICTs

“Graphene production and graphene based FET sensors”

MASTER DEGREE THESIS

Supervisors:
Matteo Cocuzza
Simone Marasso
Alessio Verna

Candidate:
Davide Benedetto Cirignola

Abstract

Graphene, the thinnest and the lightest sp2 carbon nanomaterial, has exhibited extraordinary properties in terms of fast electron mobility, high current density, high mechanical strength, excellent thermal conductivity, and large surface area. These characteristics make graphene an ideal nanomaterial for nanoelectronics, nanodevices, and nanocomposites. Graphene-based sensors, thus, have attracted great attention toward providing a novel sensor platform with high sensitivity.

Exploring the graphene growth possibilities, a chemical vapor deposition based recipe has been optimized, making it consistent and repeatable. The growth process leads to two transfer possibilities from the copper substrate to a silicon one, mediated by a PMMA solution in Anisole or by a Shellac solution in Ethanol. Each sample, both for growth and transfer stages, has been characterized with Raman Spectroscopy in order to verify the quality and defectiveness of graphene, Field Emission Scanning Microscopy to identify any unwanted residue and X-Ray Photoelectron Spectroscopy to identify any elemental residue on the graphene surface.

The results show that the graphene grown with this techniques is an high quality one, monolayer and with a low quantity of defects. Meanwhile the described transfer processes are both suitable for graphene electronic applications, as demonstrated by the construction and electrical characterization of an Electrolyte Gated Graphene Based Transistor.

Contents

Chapter 1

Introduction

The main theme addressed in this thesis concerns the research of a graphene growth recipe that is able to grant, using a Chemical Vapor Deposition system, an uniform, little defective and monolayer graphene, that could be used in the production of graphene based FET sensors. This technique exploits the peculiar property of graphene, according to which it is able to grow in monolayer shape on a Copper thin film substrate, but only when exposed to a peculiar and pressure/temperature controlled environment.

In order to exploit the electrical properties of a graphene monolayer, it is mandatory to remove the Copper layer (only useful to the growth stage) with a proper etching process and transfer the graphene on a target substrate (Silicon has been used for this experimentation). A fundamental condition is to choose a proper supporting layer, useful to sustain and protect graphene during the process. Two possible materials have been identified to perform this function: PMMA in Anisole solution and Shellac in Ethanol solution.

Every growth recipe and transfer process has been characterized with Raman spectroscopy, Field Emission Scanning Microscopy and X-Ray Photoelectron Spectroscopy. These characterizations grants the demonstration that the produced graphene is monolayer, little defective and without unwanted elemental contamination.

The graphene is going to be tested in a transistor environment in order to verify its peculiar electronic properties. To accomplish this task, an Electrolyte Gated Graphene Field Effect Transistor has been chosen. Its building procedures have been designed in order to house the graphene monolayer as conductive channel. The results show that the transistor demonstrates ambipolar behavior under the electric field effect, this is coherent with what was expected from a graphene made conductive channel, validating from the electrical point of view the growth recipe and the two transfer methods, which are both equally effective to transfer the graphene layer from the Copper substrate to the FET channel location.

Chapter 2

Graphene Overview

2.1 Graphene structure

Graphene is made of a 2-dimensional single layer honeycomb (fig. 2.1) disposed carbon atoms (fig. 2.2) that are held together by a "backbone" of overlapping sp^2 orbitals.

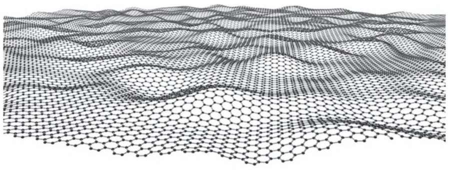

Figure 2.1: Example of graphene monolayer [1]

Each atom of this structure has four bonds: three σ bonds (strong covalent bond due to atomic orbitals overlap) with three neighbor carbon atoms and one π bond (a weak covalent bond due to partial orbital overlap) oriented out of plane. The graphene's electrical conductivity is due to the hybridized nature of the sp^2 orbitals, in which the π bonds are half-filled, permitting a huge number of free-moving electrons and owning the status of "most conductive material at room temperature" with a conductivity of $10^6\ \frac{S}{m}$.

Thanks to it's particular atomic structure, graphene results to be extremely stiff, exhibits very high thermal conductivity, has zero effective mass, is impermeable to gases and is barely optical transparent. His planar density is 0.77 $\frac{mg}{m^2}$ and his thickness (in case of a monolayer) is 0.35 nm which confers a transparency of 97.7%. The unit structure of graphene is a carbon hexagonal ring with a surface of 0.052 nm^2. This characteristics describes this material like ultra thin, ultra light and mechanically flexible but resistant.

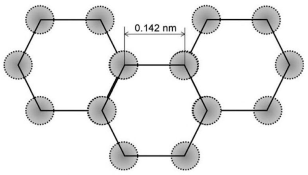

Figure 2.2: Graphene atomic structure [1]

All these properties provide graphene a huge advantage if compared with similar products both in terms of academic research and in many industrial applications, like more efficient and tunable transistor gates or by replacing traditional membranes like the indium tin oxide (ITO) one. [1, 2]

2.2 Mechanical properties

The mechanical properties of graphene are the reasons that make this material unique both as individual and as a compound agent. The high stability of the sp^2 bonds of the hexagonal lattice can oppose to in-plane deformations. A possible way to measure the mechanical properties of graphene is by nanoidentation in an atomic force microscope (AFM) (fig. 2.3), that gives the possibility to measure the breaking strength of a suspended graphene monolayer membrane, which results to be 55 Nm^{-1} (it is calculated with the force per unit width and express as Nm^{-1}), corresponding to a second order elastic stiffness equal to $E^{2D} = 340 \pm 50\ Nm^{-1}$. The correlated Young's modulus is $E = 1.0 \pm 0.1\ TPa$, assuming an effective thickness of 0.335 nm.

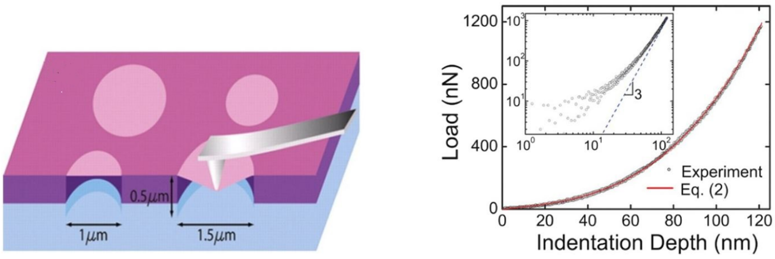

(a) (b)

Figure 2.3: Stiffness test with AFM [2], a) Nanoindentation setup in a suspended monolayer graphene membrane, b)Loading curve with increasing indentation depth

It is fundamental to specify that some reports have obtained different value of stiffness, probably due to the crumpling of sample surface in the vertical direction inducing static wrinkling, this is caused by an uneven stress at the boundary of graphene and worsen by point defects such as the "Stone-Wales" defects (fig. 2.4).

A defect-free graphene monolayer appears to be the strongest material ever tested which attests it's intrinsic strength to 130 GPa but is important to notice that a defected surface can lower significantly this value (about 60%), obtaining the same result as an high presence of wrinkles.

Another important mechanical property of graphene is the fracture toughness. According to literature, it can be measured using an *in situ* micromechanical testing device and a nanoindenter within a SEM for the determination of the fracture toughness: a central crack is induced in the middle of the monolayer membrane using a focused ion beam (FIB) and observed after applying a load. The critical strain energy release appear to be $G_c = 15.9\ Jm^{-2}$ while the fracture toughness is measured as a critical stress intensity factor $K_c = 4.0 \pm 0.6\ MPa$. From this data it can be deduced that the toughness of graphene, like other membranes, depends heavily on the weakest point where the fracture starts. [1, 2]

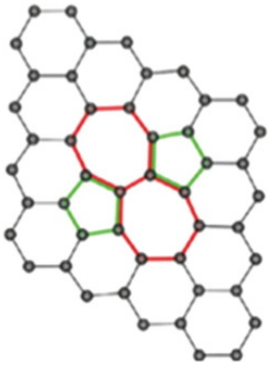

Figure 2.4: "Stone-Wales" defect in a graphene layer [2]

2.3 Graphene Preparation techniques

In the following paragraphs are listed and briefly described the most common graphene production methods. Is it easy to see that each method is quite different for quality, production cost, scalability, purity and yield of each preparation route (fig. 2.5). The most suitable way for simple laboratory experimentations results to be the chemical vapor deposition (CVD) which excels in product quality maintaining low cost and high repeatability. [2]

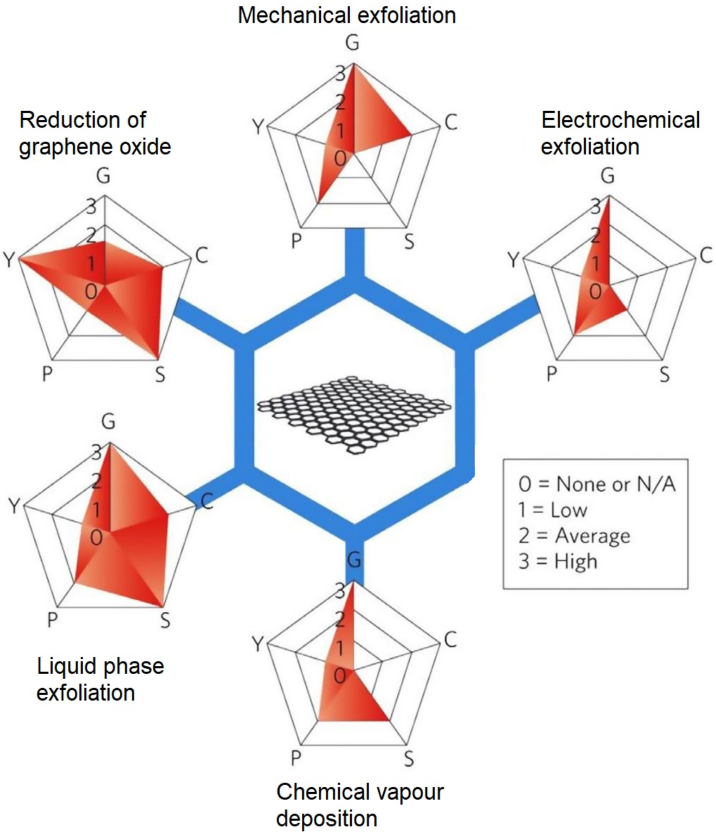

Figure 2.5: Characteristics of most common graphene production methods: (G) refers to graphene quality, (C) refers to the production cost, (S) refers to scalability, (P) refers to purity and (Y) refers to the yield [2]

2.3.1 Mechanical exfoliation

This is the first discovered and simplest way to obtain graphene. In this technique, a flake of graphite (which is composed by a lot of superimposed graphene layers, usually more than ten) undergoes repeated exfoliation by tape (fig. 2.6). In a final step, it is possible to transfer the obtained graphene to a substrate, usually silicon oxide. Due to the high unrepeatability of the results which are lacking in the predictability of the dimensions of the transferred final layer and on its actual state of monolayer, this technique is generally rarely employed in favor of other procedures. [2, 3]

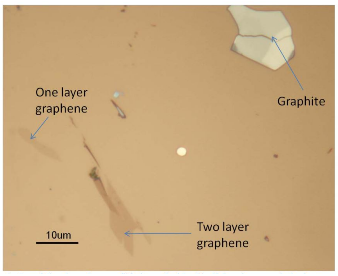

Figure 2.6: Mechanical exfoliation: from graphite to graphene [3]

2.3.2 Chemical vapor deposition - CVD

CVD is one of the simplest and most used graphene production techniques. It grants to grow a less defective and surely monolayer graphene, also called as "High quality graphene". It is also possible to tune the dimension of the growing layer, making this technique one of the best for precision and mass production, both for industrial and research purposes.

The growth mechanism is relatively simple: it consists in the exposure of a metal, usually copper but also platinum is used, to different hydrocarbon gaseous precursors at high temperature into a controlled argon and hydrogen atmosphere (fig. 2.7). The exact mechanism of graphene growth depends on the precursor metal substrate used in the process, but usually starts with the decomposition of the hydrocarbon gases at contact with the substrate surface: this brings a nucleation of carbon atoms since they regroup into larger domains forming a monolayer. [2, 4, 5]

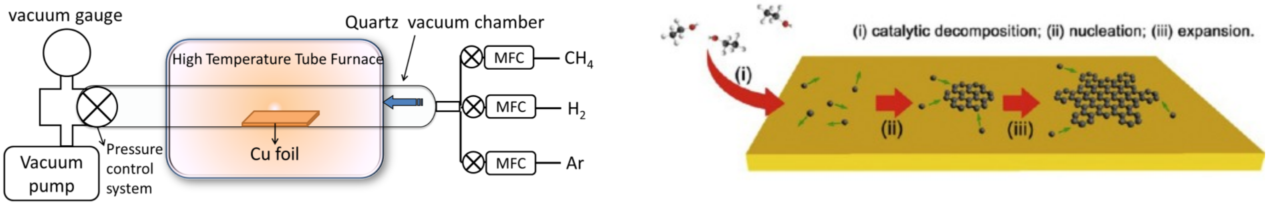

(a) (b)

Figure 2.7: Graphene CVD growth: a) Structural detail of a CVD apparatus [4], b) Graphene growth mechanism in a CVD environment [5]

2.3.3 Liquid phase exfoliation

In this technique the exfoliating action made by ultrasound is exploited in combination with an appropriate liquid solvent bath. Initially graphite flakes are submerged in a NMP ($N-methyl-2-pyrrolidone$) and sonicated in order to exfoliate the flakes. The sonication time is very important since it can tune the concentration of graphene flakes in the solution, which increases linearly with the graphite treatment time. The heavier graphite residual flakes are removed by ultracentrifugation, which is also fundamental to tune the dimension of the produced graphene flakes: higher centrifugation speed means thinner flakes (less layer) but with smaller lateral size, unfortunately not so useful in standard applications rather than composites materials.

The success of this process can be estimated over the percentage of single layer graphene produced from the total quantity of initial graphite. The process yield can be increased by an appropriate tuning of the fundamental parameters like the initial graphite concentration, the sonication time and the centrifuge speed (fig. 2.8).

This procedure is correlated with several problems, as a first instance is fundamental to notice that the high reactive solvents increase a lot the production costs while the process is not eco-friendly. In second instance is also important to notice the impossibility to evenly "wrap" a precise surface with a continuous graphene monolayer, due to its flake nature. [2, 6]

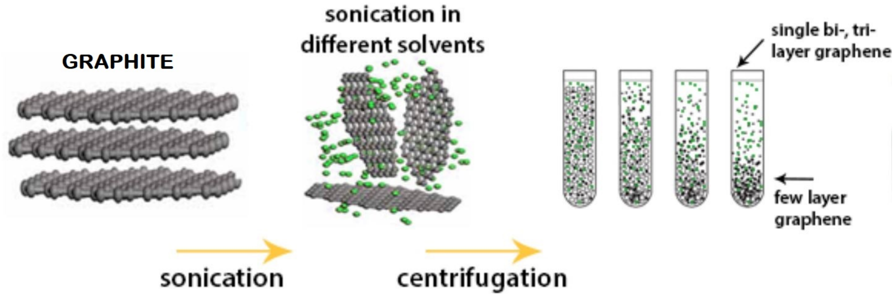

Figure 2.8: Liquid phase exfoliation process [6]

2.3.4 Electrochemical exfoliation

This production process uses a liquid electrolytic solution in combination with an electrical current to consume a graphite electrode, which will be anodic-oxidized (fig. 2.9). The resulting anodic material is composed by few graphene layers characterized by a low yield and a partial oxidation state (which is different from a pristine graphene monolayer). The lateral size of the produced flakes is dependent on the graphite source and on the condition of exfoliation process.

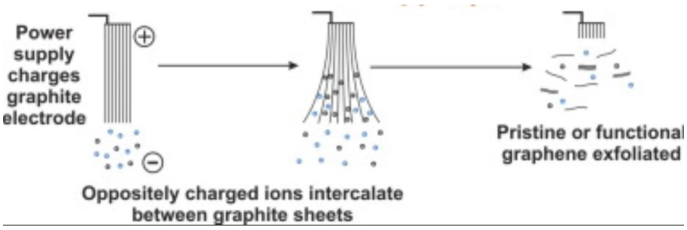

Figure 2.9: Graphene electrochemical exfoliation process [7]

The advantage of this process is that it takes place on a single step, which makes it easier to operate. It is also important to take into account that the use of liquid electrolytes or aqueous surfactants is eco-friendly, avoiding toxic and expensive chemicals which are used in most graphene preparations. [2, 7]

2.3.5 Chemical reduction of graphene oxide

The aim of this technique is to refine graphene oxide flakes previously obtained with other techniques. The chemical reduction operates in order to reduce the graphene oxide sheets into graphene-like monolayers (fig. 2.10). The choice of the solvent, the reducing agent (such as hydrazine monohydrate or hydroquinone) and the surfactant are fundamental: they must perfectly combine in order to maintain a stable suspension able to operate on every graphene oxide suspended layer and, at the end of the process, allowing the operator to pick up the product from the solution. The quality of the resulting graphene cannot be considered high since this process tends to enhance both intrinsic defects (edges and deformations) and extrinsic defects (contaminating chemical groups). It is fundamental to highlight that using such particular and dangerous reducing chemicals involves an increase of the production costs and, of course, it may be difficult to dispose of the production waste in an eco-friendly way. [2, 8]

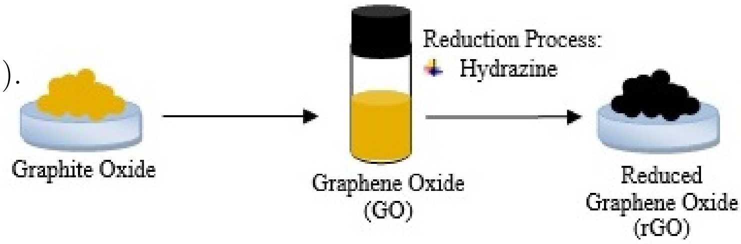

Figure 2.10: Graphene chemical reduction process [8]

Chapter 3

Graphene based Field Effect Transistor - FET - structures

3.1 Field Effect Transistor - A brief overview

A FET is an electronic device with three (or more) contacts where the conductivity between two of them, the source and the drain, is modulated by the electric field created by the third contact called gate. The gate control grants the use of a FET as switch which conducts high current when it is in ON mode and very low current when it is in OFF mode. This control is allowed by gate modulation of the free carrier density in the channel between source and drain, which is located under the gate. The ratio between current in ON mode an in OFF mode is an important performance metric: the larger, the better.

A large ON current (I_{on}) directly affects the switch on time and can be achieved improving carrier velocities through carrier mobility and thermal improvements. A low OFF current (I_{off}) is desired for low static power dissipation and can be achieved by the control of the current leaking which typically requires high band gap semiconductors (usually about 0.5 eV or more).

A FET can also be used as an analog voltage amplifier, where a signal applied to the gate modulates the channel current, which is converted to a voltage signal passing trough a resistor. There are two important parameters of a FET for both analog and rf applications: the intrinsic voltage gain and the cut-off frequency. The voltage gain depends on the transconductance $g_m = \frac{dI_{ds}}{dVgs}$ of the FET and on the resistance of the load R_L. The cut-off frequency $f_T \propto \frac{g_m}{C_g}$, with C_g intended as gate capacitance, is defined as the frequency at which the gain is unitary. The intrinsic gain can be improved using FETs with large transconductance, achieved by a channel material with high mobility.

Scaling the FETs dimensions is useful to improve performance metrics for the logic devices such as speed of operation, low voltage and low power operation. Shrinking the gate length results in a reduction of the gate control on the channel. The lack of control can be countered by increasing the channel doping, this procedure leads to a reduction of the carriers mobility due to increased scattering events, affecting the overall performance of the device. Using a graphene gate makes possible to overcome the performance reduction allowing a scaled device without the main drawbacks. [9]

3.2 Graphene Field Effect Transistor - GFET

The silicon-based electronic is tending to its scaling limit, so the industry is looking for a material that can replace the classic silicon field effect transistor (FET). Graphene, with its exceptional electronic properties, can be processed maintaining the conventional technology already used for planar architectures (CMOS-like structures), giving a serious advantage with respect to the commonly used semiconductor materials to which it can offer a substantial alternative. Another fundamental property is the quality of graphene-substrate and graphene-insulator interface: since graphene is a single atomic layer thick, the carriers are always adjacent to these surfaces, minimizing the scattering sources and achieving very high performance FETs. Also, due to very high mobility of electrons in graphene, it offers high advantages as a channel material, it also counter the loss of electrostatic control and short channel effects resulting from scaling. In addition to these advantages and thanks to the large mobility of carriers and high current carrying capability (near to $10^8\ Acm^{-2}$), graphene could also be useful for application in radio frequency circuits. However, the major drawback to the use of graphene is its near zero band gap, which make the graphene-based FETs hard to switch off (poor $\frac{I_{on}}{I_{off}}$ ratio) and problematic for logic applications.

The fabrication of a graphene field-effect transistor (GFET) can be summed up in three major steps: preparation of a substrate that can host graphene, deposition of gate dielectric and forming contacts between metal and graphene. This steps are also the representation of the critical interfaces: graphene-substrate, graphene-dielectric and metal-graphene.

After the preparation of a substrate with graphene on it, is necessary to deposit an insulating layer. For the correct working of the GFET system, a small gate capacitance C_g is needed, therefore is mandatory to use low leakage, thin and uniform high-k (dielectric constant) dielectric, usually deposited by thermal evaporation or atomic layer deposition (ALD).

Another critical interface in GFET is the graphene-metal interface: metal contacts can be created by electron bean lithography followed by electron beam evaporation of the metal and lift-off, usually metals like Titanium (Ti), Gold (Au), Chromium (Cr), Platinum (Pt), Nickel (Ni) and Cobalt (Co) are used since they have an high work function and they can reach a specific contact resistance in a range of values between 500 and 4000 $\Omega\mu m$. [9, 10]

3.2.1 GFET capacitance-voltage characteristics

Is possible to evaluate the capacitance related to the gate with a simple model that can explain the gate control over the channel charge: it is convenient to consider a series of two capacitors, one represents the geometrical capacitance of the gate and the other represents the quantum

capacitance of graphene. The quantum capacitance $C_q = \frac{\partial Q}{q \partial E_F}$ is related to the density of states of the conductors used for the FET structure. Since graphene is a bi-dimensional low density of states material, as the carriers start moving, they tend to occupy high energy states leaving behind less energetic electrons in the low energy states. The band filling/emptying effect alters the gate capacitance which results to be the sum of quantum and geometrical capacitances. Therefore quantum capacitance represents the extra voltage required to modulate the charge density for a fixed electrostatic potential (fig. 3.1).
Using this model is possible to obtain the dependence of the channel charge on the gate voltage.

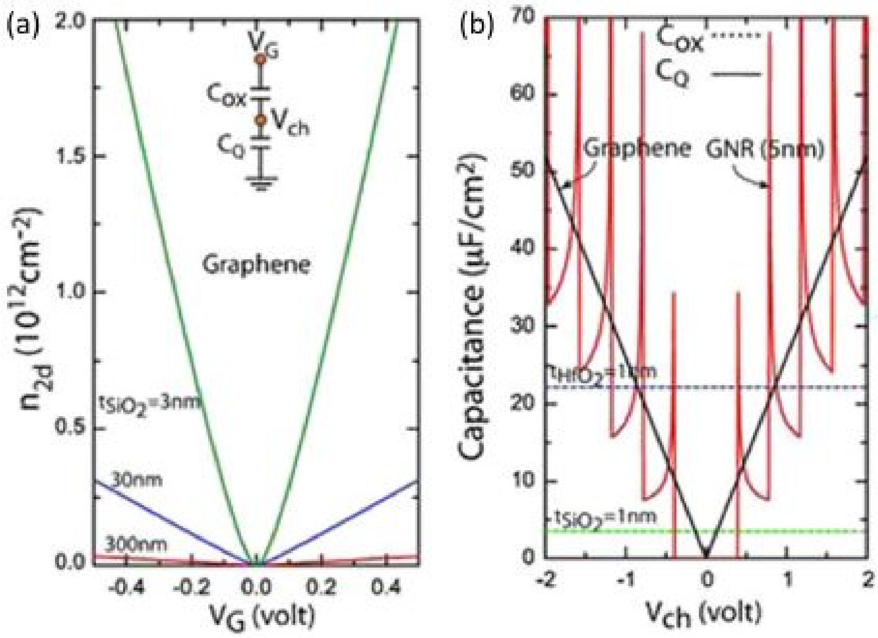

Figure 3.1: a) 2D carrier density in graphene as a function of gate voltage for different oxide thickness. b) Quantum capacitance of 2D graphene and a 5 nm GNR compared with the parallel-plate capacitance of a 1 nm SiO_2 and HfO_2 [9]

As it is possible to see, for an oxide effective thickness approaching 1 nm, the quantum capacitance of graphene becomes comparable or less than the oxide capacitance, reducing the benefits of an effective oxide thickness decrease. Thus, the small quantum capacitance of graphene can negatively impact the device performance. [9, 10]

3.2.2 GFET current-voltage characteristics

The bulk graphene-based FETs have mobilities much larger than similar conventional FETs (mostly due to the near zero graphene bandgap) so the ON/OFF current ratios are usually less than 10. It is fundamental to keep in mind that the working principle of a FET is the possibility to modulate the charge density in the channel, so in total absence of chemical doping, the gate voltage at the minimum current will match the flat-band voltage V_{FB} which is related to the Fermi level into the Dirac point. For $V_G > V_{FB}$ the Fermi level sits in the conduction band and the shape of the right side $I - V$ characteristic is due to the conduction of electrons, whereas for $V_G < V_{FB}$ the Fermi level is in the valence band and the shape of the left side $I - V$ characteristic is due to conduction of holes (fig. 3.2). With V_G near to V_{FB} there is presence of both kind of carriers and then the conductivity of graphene is minimized.

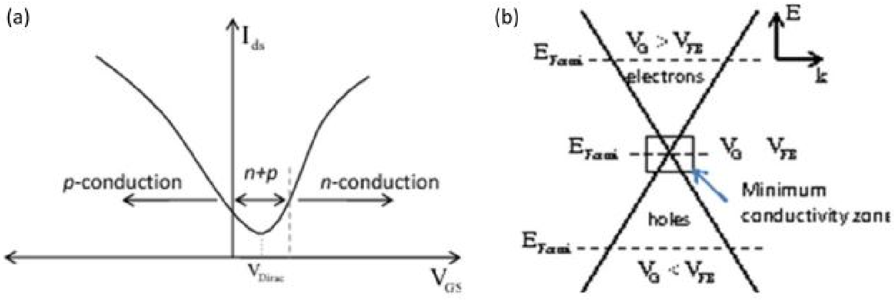

Figure 3.2: a) Schematic of a typical characteristics of a graphene based FET. b) Schematic of band energy diagram showing the Fermi level for electron, hole and minimum conductivity zones. [9]

However there is always a thermal distribution of carriers and fluctuation of energy at the Dirac point, so the minimum current remains significant at $V_G = V_{FB}$ even when the system is cooled down to very low temperatures.

Another typical property of transfer characteristics of GFETs is the asymmetry between the electron and hole conduction. This behavior is attributed to a geometry-dependent combination of some V_G-dependent contact resistances which lead to the formation of $p - n$ junctions between the channel and the source and drain regions (for only $V_G < V_{FB}$ or only $V_G > V_{FB}$ depending of p-type or n-type source/drain regions).

The saturation current condition in a GFET architecture is difficult to reach. While in conventional MOSFETs the possible mechanism for current saturation are the pinch-off and velocity saturation, in a GFET structure the first method can't be used. Therefore, in order to drive the device into a saturation regime the drain-to-source electric field must be high enough to cause velocity saturation. In devices with poor contacts, significant voltage is dropped across the connections, increasing the difficulty to drive the device into saturation. Consequently is very rare to see true saturation characteristics, as the quality of graphene increase to achieve higher mobility, it becomes even more necessary to improve the contact quality to observe true saturation behavior. [9, 10]

3.3 Electrolyte gated GFET

In the biological sensors research, a FET-based approach offer the possibility to make cheap, stand-alone, and small (implantable solution) sensors with greatly simplified readout systems. Moreover, FET-based graphene sensors, due to the increased performance and to the inertness of graphene, enables a direct and effective interface with many chemical and biological environments. This is particularly beneficial for the electrolytic environments present in a great variety of biological and chemical sensing applications because graphene can exploit the electrical double layer phenomenon and resulting ultrahigh interface capacitance. [11, 12]

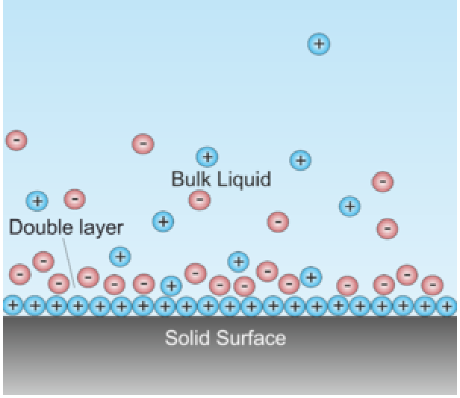

Figure 3.3: Schematic of electrical double layer in a liquid at contact with a negatively-charged solid. Depending on the nature of the solids, there may be another double layer (unmarked on the drawing) inside the solid.

The electrical double layer (DL) is a structure that appears on the surface of an object when it is exposed to a fluid, it consists in two parallel layers of charge surrounding the object (in this case, the graphene layer). The first layer, called surface charge, consists of ions adsorbed onto the object due to chemical or physical interaction. The second layer is composed of ions attracted to the surface charge via Coulomb force, this layer is loosely associated with the object since it is made of ions free to move in the fluid under the influence of electric attraction and thermal motion rather than be firmly anchored (fig 3.3). The large capacitance granted by the electrical double layer coupled with graphene's high mobility enables high-transconductance FET sensors.
Graphene electrolyte-gated field-effect transistors (EGFET) consists of a graphene channel between two conductive source-drain contacts, which are typically metals. Some portion of the graphene channel is exposed to the electrolytic environment (fig. 3.4). This allows changes in the electrolytic environment to alter the graphene channel's electrical properties. Some form of read out circuitry is then used to identify these changes in electrical properties. No material constraints are imposed on the substrate, which can vary from glass to silicon to polymer.[11, 12]

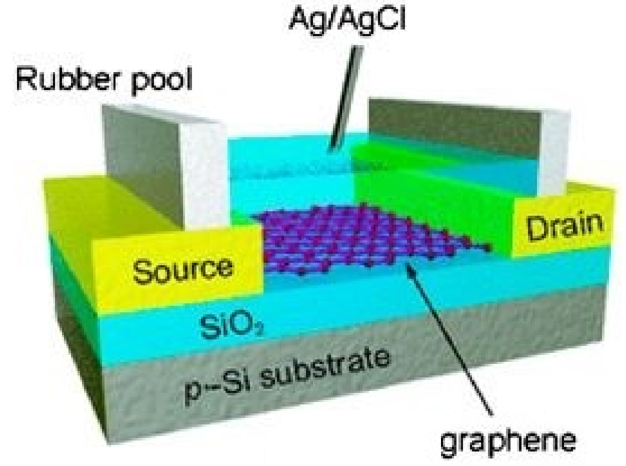

Figure 3.4: Electrolyte Graphene Field Effect Transistor schematics [11]

Graphene electrolyte-gated field-effect transistor (EGFET) sensors rely on one of two operation principles: Dirac point shifts or V_{GS} modulation (fig. 3.5). In the Dirac point shift approach, a change in the electrolytic environment alters the graphene Fermi level. For other applications, graphene EGFETs can be operating based on V_{GS} modulation: the change in the effective V_{GS} results in a detectable change in I_{DS} current.[11, 12]

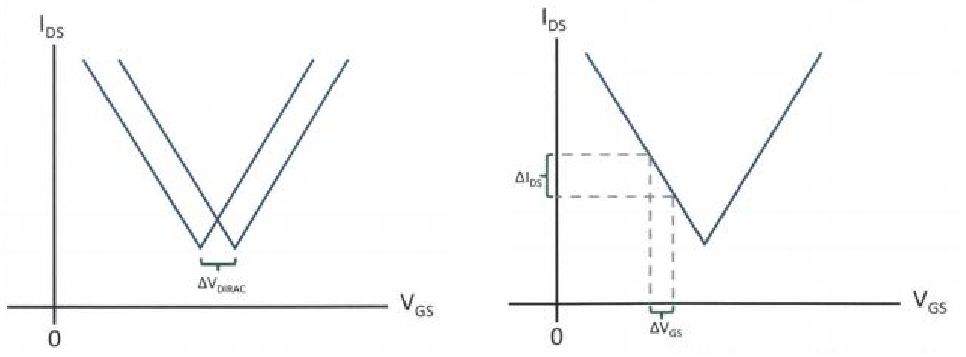

(a) Changes in electrolyte composition alters graphene doping and the location of Dirac point [12]

(b) Chang in ionic composition near graphene surface modulates the applied V_{GS} voltage [12]

Figure 3.5: Graphene CVD growth

Chapter 4

Technologies used to produce and characterize graphene samples

4.1 Production Technologies

4.1.1 Nano Chemical Vapor Deposition - CVD

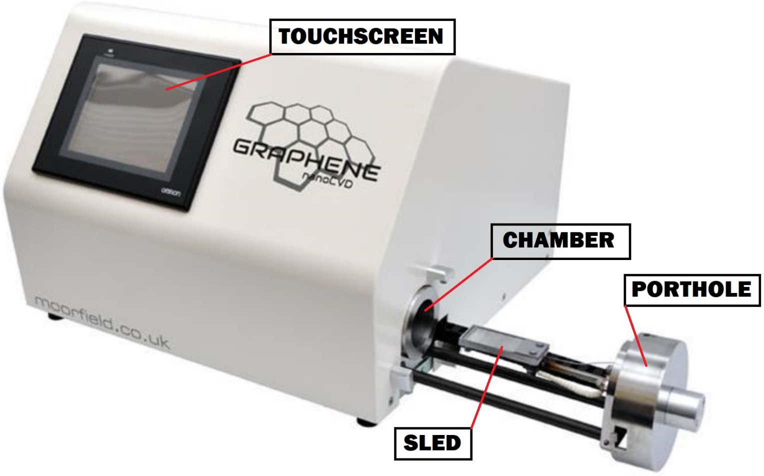

Figure 4.1: *Moorefield nanotechnology nanoCVD-8G*, sidelong view

As mentioned before (Chapter 1.3), the chemical vapor deposition (CVD) is one of the simplest and most effective techniques for graphene production. This technology has been used for its capacity to produce high quality monolayer graphene with little effort, resources and in restricted times.

All the graphene samples were grown using a benchtop *Moorefield nanotechnology nanoCVD-8G* (fig. 4.1). This particular CVD system is composed by a plastic body that house a pressure/temperature controlled chamber, which is connected to four gas inlet (each one controlled by an electronic valve) ad to an electric rotary vacuum pump. On the front panel (fig 4.2) is possible to see a touch screen which allows the operator to control the system status, and set all the fundamental parameters in order to define the graphene growing style.

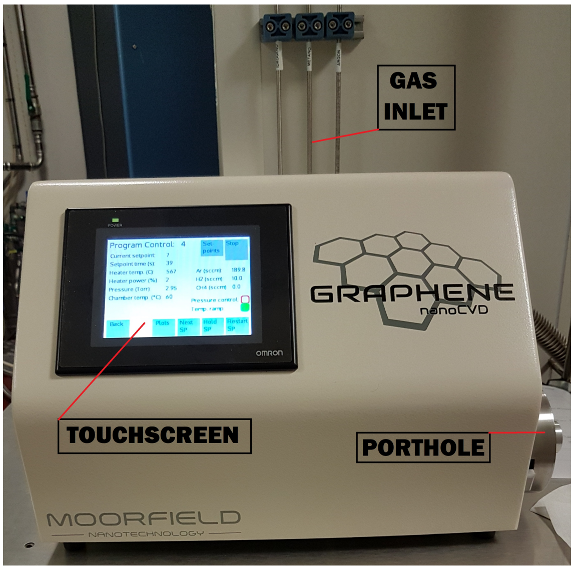

Figure 4.2: *Moorefield nanotechnology nanoCVD-8G*, front view

On the right panel there is the chamber porthole through which is possible to inspect the inside of the chamber and the sled that will house the samples. On the back side there are the electrical network connection and the gas line connections. Through the user interface, in addition to selecting the growth settings in temperature and pressure, is possible to check in real time the correct performance of the growth operation with the help of a complete set of graphs updated every three seconds.

4.1.2 Electron-beam Physical Vapor Deposition - EBPVD

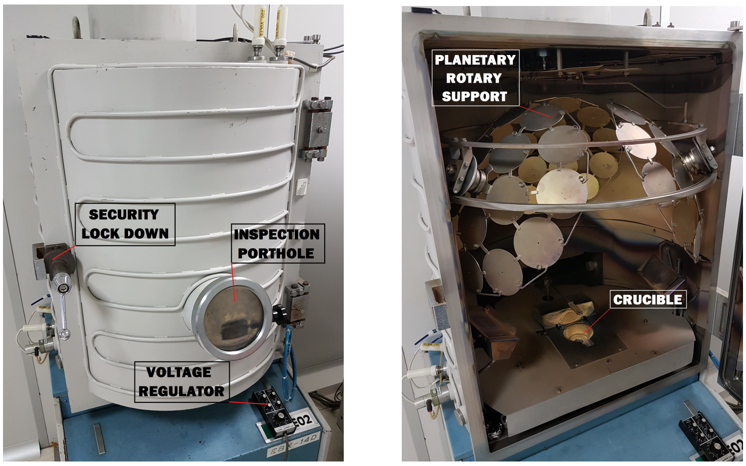

(a) (b)

Figure 4.3: *ULVAC EBPVD*, front view. a) chamber door, b) Chamber inside front view

Electron-beam Physical Vapor Deposition (fig. 4.3) is a particular way to perform a physical vapor deposition. A target anode is bombarded, using an electron beam given off by a charged tungsten filament under high vacuum. The electron beam causes atom from the target to transform into gaseous phase, in order to precipitate into solid form, coating everything in the anode line of sight.
During the deposition, the chamber must be evacuated to a pressure of at least $7.5 \cdot 10^{-5}\ Torr$ to allow the passage of electrons from the gun, generated by thermionic emission and accelerated by an high kinetic energy to the evaporation material, which is in ingot form (fig. 4.4). When electrons hits the evaporation material, they will lose energy which is converted to a thermal one, heating the ingot. The resulting vapor is used to coat surfaces.
The samples are placed into the planetary rotary support, its particular rotative movement aim to grant an uniform deposition avoiding blind spots.

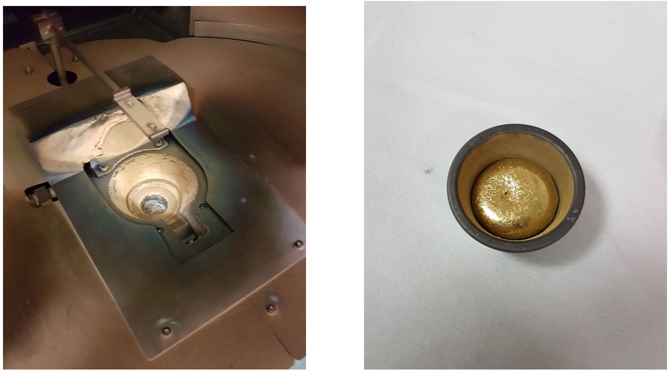

(a) (b)

Figure 4.4: *ULVAC EBPVD*. a) Crucible detail, b) Ingot detail

4.1.3 Mask aligner

Photolithography is a process used in microfabrication to selectively remove parts of a thin film (or the bulk of a substrate). It uses UV light to transfer a geometric pattern from a photomask to a light-sensitive chemical (photoresist) on the substrate.

A series of chemical treatments then engraves the exposure pattern into the material underneath the photoresist. In a complex integrated circuit (for example, modern CMOS), a wafer will go through the photolithographic cycle up to 50 times.
It is important to mention that the positive photoresist, the most common type, becomes soluble in the basic developer when exposed, meanwhile the negative photoresist becomes insoluble in the developer. This chemical change allows some of the photoresist to be removed.
The image for the photomask originates from a computerized data file. This data file is written onto a square fused quartz substrate covered with a layer of chrome. A laser writer uses a laser beam to expose the pattern defined in the data file and travels over the surface of the substrate in either a vector or raster scan manner. Where the photoresist on the mask is exposed, the chrome can be etched away, leaving a clear path for the light in the stepper/scanner systems to travel through.
The mask aligner (fig. 4.5) is the instrument that grant to align the photomask with the substrate in order to pattern the correct area (it may be useful to align the pattern with already present features), this operation is made possible using a couple of optical lenses that are able to magnify and align the features on both photomask and substrate. After the alignment procedure, the mask aligner is able to expose the photoresist on the substrate with an UV light of predetermined intensity for a precise period of time. After the exposure, the photoresist is ready to be developed.

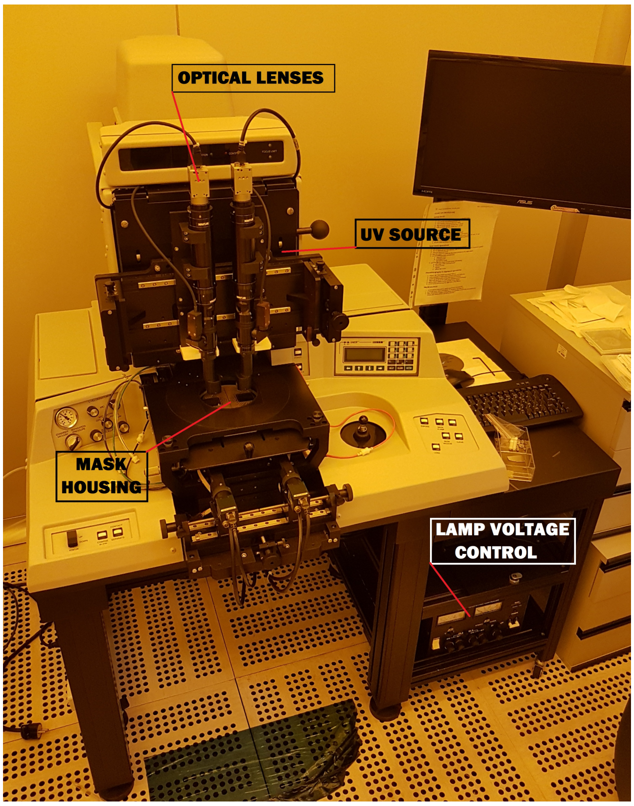

Figure 4.5: Laboratory Mask Aligner, front view. The yellow light is due to the class 100 clean room illumination

4.2 Characterization technologies

4.2.1 Raman spectroscopy

Figure 4.6: *Renishaw inVia confocal Raman microscope*, front view

The Raman spectroscopy (fig. 4.6) is a technique used to obtain a ”structural fingerprint” That can be used to identify molecules and elements. It relies on inelastic scattering (Raman scattering) of monochromatic light emitted from a laser (fig. 4.7). The laser light interact with molecular vibrations and phonons resulting in an emitted photon energy shift. The energy shift gives information about the vibrational modes in the system. When the sample is illuminated with a laser beam, an electromagnetic radiation from the illuminated spot is collected with a lens, sent through a monochromator and than filtered in order to remove Rayleigh scattering events.

Figure 4.7: *Renishaw inVia confocal Raman microscope*, side view

The magnitude of the Raman effect is correlated with the polarizability of the electrons in a molecule. It is a form of inelastic light scattering in which a photon excites the sample, this excitation brings the molecule into a ”virtual” energy state for a short time before the photon is emitted. Inelastic scattering means that the energy of the emitted photon could be lower or higher than the incident photon energy. After the scattering event, the sample is in a different rotational or vibrational state. In order to keep the total system energy constant, the scattered photon shifts to a different energy, and therefore a different frequency. If the final state is higher in energy than the initial state, the scattered photon will be shifted to a lower frequency (lower energy) so that the total energy remains the same. This shift in frequency is called Stokes shift, or downshift. If the final state is lower in energy, the scattered photon will be shifted to a higher frequency, which is called anti-Stokes shift, or upshift.

Raman spectroscopy is used to identify molecules and elements and to study chemical bonding. Since vibrational frequencies are specific to a molecule's chemical bonds, Raman provides a "fingerprint" to identify molecules and elements. In solid-state physics, Raman spectroscopy is used to characterize materials and find the crystallographic orientation of a sample. Like with single molecules, a solid material can be identified by characteristic phonon modes, so the informations on the population of a phonon mode are given by the ratio of the Stokes and anti-Stokes intensity of the Raman signal.

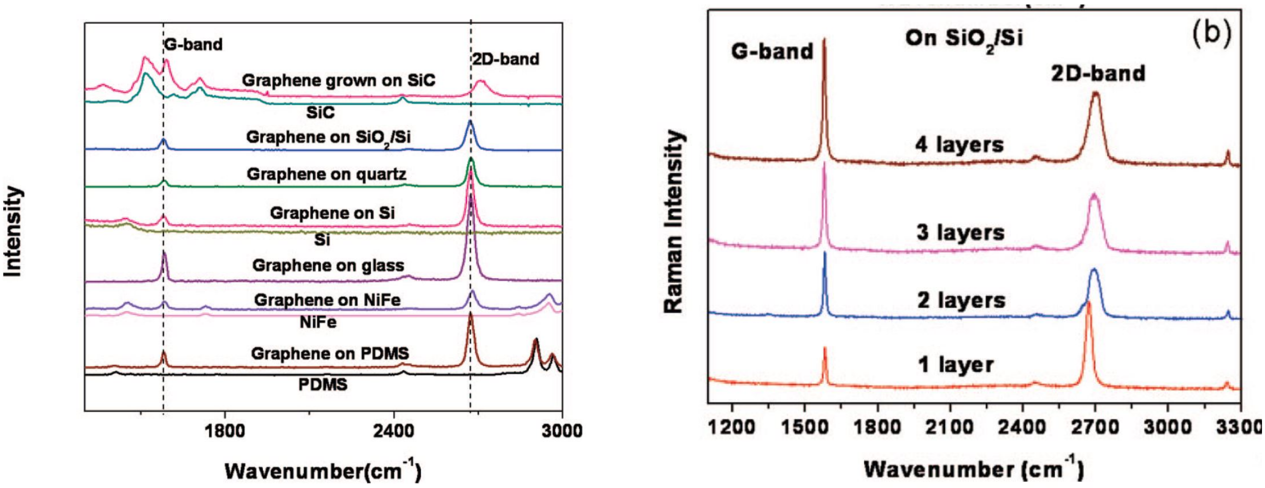

(a)

(b)

Figure 4.8: a) Raman spectra of monolayer graphene on different substrates [13], b) Raman spectra of a monolayer, bilayer, three layers and four layers graphene on SiO_2/Si [13]

The Raman spectroscopy provide useful information regarding graphene (fig. 4.8), such as the defects (D-band), in-plane vibration of sp^2 carbon atoms (G-band) and stacking orders (2D-band). The graphene monolayer can be unambiguously identified by Raman spectroscopy from his characteristic 2D band, symmetrical and sharp shaped. Also analyzing the G-peak intensity is possible to obtain more information regarding the graphene structure: the greater G-peak intensity is (compared with the 2D peak intensity), the more layers the graphene will have. Another important information is that regardless of the substrate, the graphene raman spectra will generally be always similar, both in peaks shapes and amplitudes. The only exception occur with silicon carbide (SiC) as a substrate.

The G-band and the 2D-band position for the Si substrate, sits around respectively at $1580 cm^{-1}$ and $2672 cm^{-1}$ with full width at half-maximum respectively around $16 cm^{-1}$ and $28 cm^{-1}$. This values are very similar for graphene transferred on SiO_2 $300 nm$ thick/Si, quartz, Si, glass, NiFe and PDMS substrates.[14, 15, 16]

4.2.2 Field Emission Scanning Electron Microscopy - FESEM

The Field Emission Scanning Electron Microscope (FESEM) (fig. 4.9) is an instrument which provides a wide variety of information from the sample surface, with high resolution and a great energy range. The characterization consists in the scanning of the sample surface with an electron beam, while a monitor displays the required information based on the detectors in use.

As a source of electrons, the FESEM uses a field emission gun that provides extremely focused electron beams, both on high or low energy. This peculiarity greatly improves the spatial resolution and grants the possibility to perform analysis at very low potentials (from 0.02 to 5 KV), helping to minimize the charging effect on non-conductive samples and to avoid damage to sensitive samples. The equipment in operation is the *ZEISS Supra 40 Field Emission Scanning Electron Microscopy*, incorporating the following detectors:
An X-Ray Dispersive Energy Detector which receives x-rays from each surface point the electron beam passes over. As the x-rays scattered energy is a characteristic of each chemical element, it provides qualitative and quantitative analytical information about selected points, lines, or areas on the surface of the sample. This technique is known as Microanalysis by EDS.
A Secondary Electron Detector, which provides a SEM topography image of the sample surface with a large depth of field. It is mainly used to browse the sample at low magnification in search of points of interest and to study samples with a large amount of topographic information.
A Backscattered Electron In-lens Detector which provides a pure backscattered signal with no secondary electron contamination and very low acceleration potential. It gives a high Z-contrast. It is also capable of working at very low voltage, which makes it ideal for sensitive samples.
A Backscattered Electron Detector which is used to observe changes in the chemical composition of a specimen. This detector permits selection of images with topographic and compositional contrast. Moreover, its high-angle working mode allows us to observe structural contrast in crystalline samples.

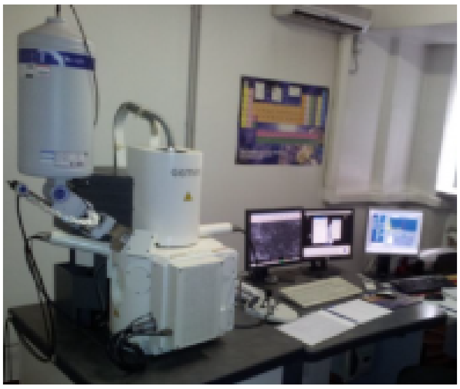

Figure 4.9: *ZEISS Supra 40 Field Emission Scanning Electron Microscopy*, front view

4.2.3 X-Ray Photoelectron Spectroscopy - XPS

X-ray photoelectron spectroscopy (XPS) (fig. 4.10) is a surface-sensitive quantitative spectroscopic technique that measures the elemental composition of a material. XPS spectra are obtained by irradiating the sample with a beam of X-rays and, simultaneously, measuring the kinetic energy and number of electrons that escape from the specimen top layer. XPS requires high vacuum (from 8 to 10 millibar) conditions.

A typical XPS spectrum is a plot of the number of electrons detected (Y-axis, ordinate) versus the binding energy of the electrons detected (X-axis, abscissa). Each element produces a characteristic set of XPS peaks at precise binding energy that directly identify each element that exists on the surface of the sample. These characteristic spectral peaks correspond to the configuration of the electrons within the atoms. The number of detected electrons in each of the characteristic peaks is directly related to the quantity of element in the sampling volume. To generate atomic percentage values, each raw XPS signal must be corrected by dividing its signal intensity (number of electrons detected) by a "relative sensitivity factor" (RSF), and normalized over all of the elements detected.
XPS could detects only those electrons that are escaped from the sample into the vacuum of the instrument, and reach the detector. Photo-emitted electrons can suffer of inelastic collisions, recombination or trapping within the material, all of this events could reduce the number of escaping photoelectrons. These effects appear as an exponential attenuation of the signal as the measurement depth (from the sample surface) increases, making the signals detected from the sample surface much stronger than the signals detected from below it.

Figure 4.10: *DISAT* XPS equipment

4.2.4 Transmission Electron microscopy - TEM

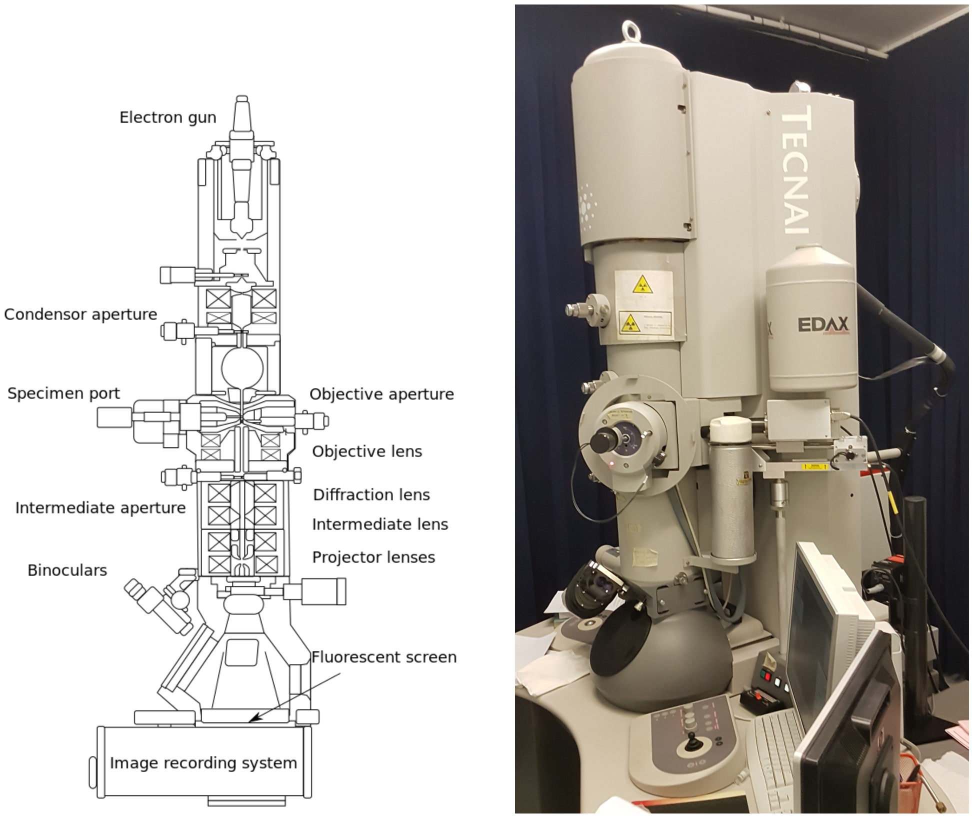

(a) (b)

Figure 4.11: Comparison between TEM schematics and TEM physical appearance. a) TEM schematics. b) *FEI Tecnai G2 F20 ST FE-TEM*, Side view

Transmission electron microscopy (TEM) is a microscopy technique in which a beam of electrons is transmitted through a sample to form an image. The sample must have a section thinner than 100 nm and needs to be suspended on a grid. The image is generated from the interaction of the electrons with the sample when they pass through the specimen. Then occur magnification and focusing into an imaging device, like a fluorescent screen. Transmission electron microscopes can produce images at a significantly higher resolution than classic light microscopes, this enables the instrument to capture detail small as a single line of atoms. At lower magnifications TEM image contrast is due to differential absorption of electrons by the material due to differences in composition or thickness of the material.
From the top down (fig. 4.11), the TEM consists of an emission source, which is a tungsten filament. The gun is connected to an high voltage source (from 100 to 300 KV) that will allow to emit electrons either by thermionic effect or field electron emission. The upper lenses of the TEM then focus the electron beam to the desired size and location. Manipulation of the electron beam is performed using magnetic and electrostatic fields: the interaction of electrons with a magnetic field will cause electrons to move according to the left hand rule, allowing for electromagnets to manipulate the electron beam.

Moreover, electrostatic fields cause the electrons to be deflected through a constant angle. From these two effects, as well as the use of an electron imaging system, sufficient control over the beam path is possible in order to grant the correct functioning of the instrument. The optical configuration (fig. 4.12) of a TEM can be rapidly changed since lenses in the beam path can be enabled, changed in their action on the beam, or be entirely disabled via electrical switching.

The lenses of a TEM allow for beam convergence, with the angle of convergence as a variable parameter, allowing to change magnification by modifying the amount of current that flows through the coil and lenses. Typically a TEM consists of three stages of lensing which are: the condenser lenses, the objective lenses, and the projector lenses. The condenser lenses are responsible for primary beam formation, while the objective lenses focus the beam that comes through the sample itself, the projector lenses are used to expand the beam onto the phosphor screen. The magnification of the TEM is due to the ratio of the distances between the sample and the image plane. Stigmators allows for the correction of asymmetrical beam distortions, known as astigmatism.

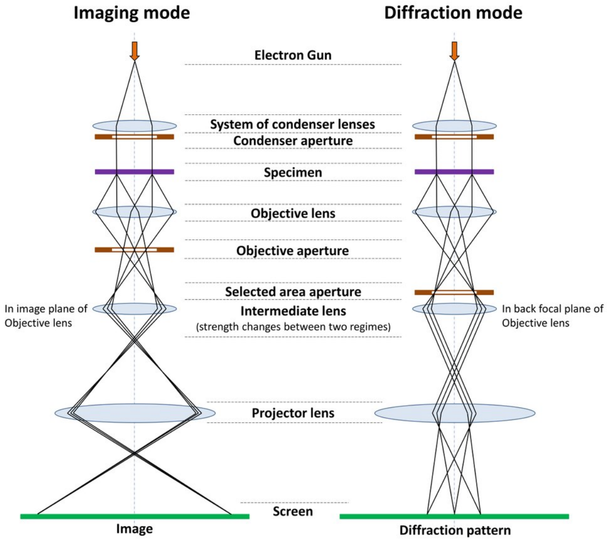

Figure 4.12: TEM imaging schematics

(a) (b) (c)

Figure 4.13: From the grid to the sample holder housing. a) TEM sample grid, b) TEM grid holder, c) Grid holder housed in operating TEM

To increase the mean free path of the electron, the TEM works on low pressures (10^{-4} Pa), such a low pressure is required for two reasons: the tolerance for the voltage difference between the cathode and the ground in order to not generate an arc, and to reduce the collision frequency of electrons with gas atoms. Poor vacuum in a TEM can cause several problems ranging from the deposition of gas inside the chamber to more severe cathode damages caused by electrical discharge.

The TEM design include airlocks to allow for insertion of the sample holder into the vacuum with minimal loss of pressure in other areas of the microscope. The sample holder (fig. 4.13), hold a standard sized sample grid. Standard TEM grid sizes are 3 mm diameter, with a thickness and mesh size around 100 μm on which the sample is placed. Usual grid materials are copper, molybdenum, gold or platinum. After the preparation, the grid is placed into the sample holder, which is inserted inside the TEM. The sample has to be manipulated in order to locate the region of interest to the beam, so the TEM stage allows for movement of the sample in the XYZ space.

Chapter 5

Graphene growth and Transfer

5.1 Graphene growth

According to literature [17], the simplest and most effective way to grow monolayer graphene is by Chemical Vapor Deposition on a thin catalytic copper substrate. The copper foil has been cut from a coil in 20 *mm* edged squares in order to fit the *Nano CVD* slit. It is fundamental to use a thin copper foil in order to simplify the future etching operations, so it was chosen a $25 \mu m$ thick copper 99% pure (*GOODFELLOW copper coil*) (fig. 5.1). The copper foil must be the least crumpled possible, if the substrate has "wrinkle defects", the up-growing graphene will be highly defective in turn, nullifying all the precautions implemented in order to obtain a monolayer.

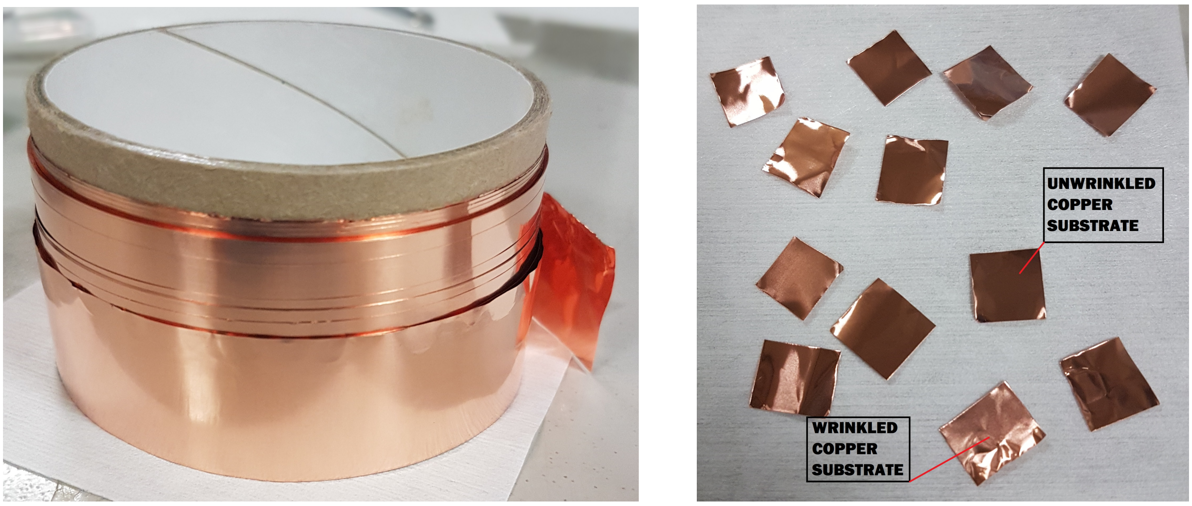

(a) (b)

Figure 5.1: Copper from coil to square samples. a) Copper foil coil, b) Copper square cut samples

The thin oxide layers on Copper, which is naturally formed at room temperature at atmospheric conditions, should be removed prior to graphene growth [18]. In order to perform this cleaning action (fig. 5.2) it is possible to exploit the chemical reaction between Hydrochloric acid and Copper oxide:

$$CuO(s) + 2HCl(aq) = CuCl_2(aq) + H_2O(l)$$

Copper does not react with hydrochloric acid, but copper oxide does: a metal-acid reaction is always a redox one, but since copper has an higher reduction potential than hydrogen, it does not react with non-oxidizing acids like HCl. Metal oxides are basic substances, so they generally react with acids forming the respective salt and water (neutralization reaction). Copper oxide is a weak base and it easily reacts with hydrochloric acid forming copper chloride and water.
In order to remove the oxide from the substrate it is necessary to prepare an hydrochloric acid solution diluted at $30\%_{vol}$ in water (*SIGMA ALDRICH HCl 36.5% - 38%*) and to immerse the copper in it for twenty minutes.

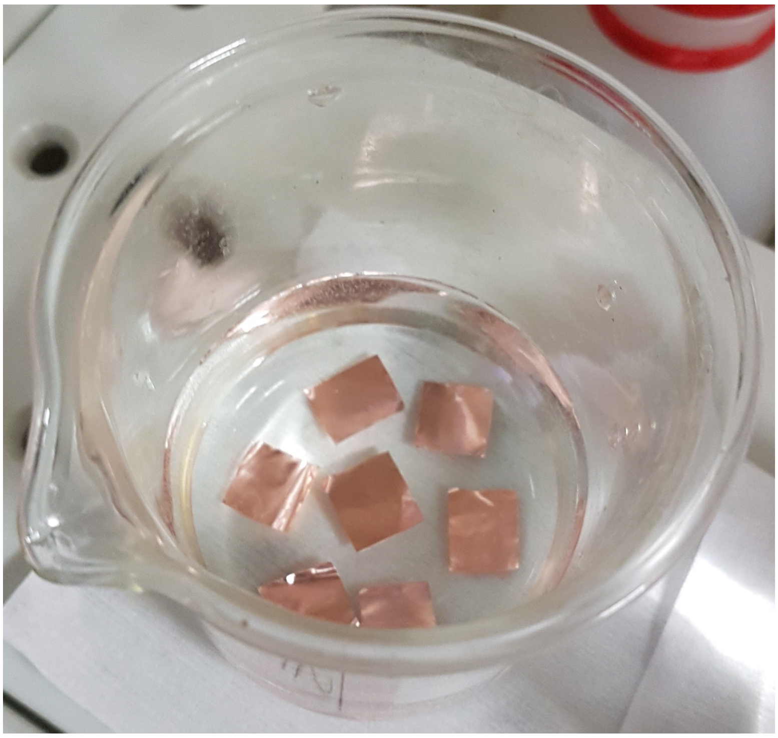

Figure 5.2: Copper samples immersed into hydrochloric acid solution

After the twenty minutes of cleaning process, each copper sample must be rinsed in clean deionized water and then meticulously dried with gaseous nitrogen. The drying phase is crucial since every water residue will oxidize the foil, making the cleaning process useless.

When the *Nano CVD* instrument is powered up, the system will autonomously start a chamber cleaning process (chamber purge process), in which Argon is injected at different pressures in order to remove all residues of previous processes. Opening the chamber porthole expose the slid that will house the samples (fig. 5.3), is important to not overload the slid in order to allow a correct circulation of the injected gases.

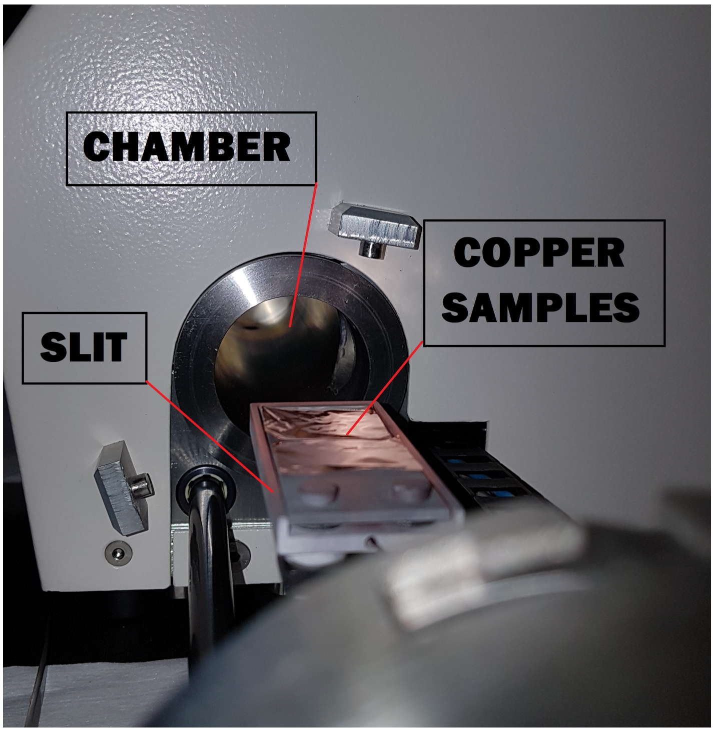

Figure 5.3: Copper samples housed onto the chamber slit

In order to achieve a monolayer graphene growth it is fundamental to design all the stages of the process that will take place inside the chamber: Initially, the slit is heated up until reaching a temperature of 1000 ℃, slightly below the copper melting point, in a constant Argon and hydrogen gas flowing atmosphere. The system pressure is then stabilized and gaseous methane is injected in the chamber, starting the graphene growing stage. In the final stage, the copper substrate is cooled down to room temperature. It is fundamental to notice that the duration of the growing stage and the atmosphere of the cooling down stage are crucial in order to achieve a correct growth: if the copper substrate takes too much time to cool down from working temperature to ambient temperature or if the graphene growing stage lasts too long, the resulting graphene will develop multi-layer islands on his surface. [19]
In order to optimize the process to obtain the less defective growth, four different growth process flow have been tested, as reasonable only one of them gave the best result. In the following will be briefly presented the difference between the four process and then only the best one will be studied in deep.

- **Recipe 1**: The first sample has been subjected to a growth stage of 300 seconds at 1000 ℃. During this stage, the total atmosphere pressure was 10 torr, divided in 80% Ar, 10% H_2 and 10% CH_4. After the growth process, the sample was cooled down to room temperature in an argon atmosphere.
- **Recipe 2**: The second sample has been subjected to a growth stage of 300 seconds at 1000 ℃. During this stage, the total atmosphere pressure was 10 torr, divided in 80% Ar, 10% H_2 and 10% CH_4. After the growth process, the sample was cooled down to room temperature in an argon and methane atmosphere.
- **Recipe 3**: The third sample has been subjected to a growth stage of 120 seconds at 1000 ℃. During this stage, the total atmosphere pressure was 10 torr, divided in 80% Ar, 10% H_2 and 10% CH_4. After the growth process, the sample was cooled down to room temperature in an argon atmosphere.
- **Recipe 4**: The fourth sample has been subjected to a growth stage of 120 seconds at 1000 ℃. During this stage, the total atmosphere pressure was 10 torr, divided in 80% Ar, 10% H_2 and 10% CH_4. After the growth process, the sample was cooled down to room temperature in an argon and methane atmosphere.

	Growth time	Cooling atmpsphere
Sample 1	300 s	Argon
Sample 2	300 s	Methane
Sample 3	120 s	Argon
Sample 4	120 s	Methane

Samples summary table

The process that give the best result in term of growing the less defective monolayer graphene is the fourth (see par. 5.0.1) that will be now studied in deep:

1. The slit heat the copper sample ramping up from ambient temperature to 900 ℃, the chamber is filled with a gas flow of: 190 sccm Argon, 10 sccm Hydrogen.
2. The temperature is kept stable to 900 ℃ for 120 seconds, the gas flow into the chamber is unchanged: 190 SCCM Argon, 10 SCCM Hydrogen. This stage aims to ensure that all the sample mass reach the target temperature.
3. the temperature is raised to 1000 ℃ which is the optimal value for graphene growth, the gas flow into the chamber is unchanged: 190 SCCM Argon, 10 SCCM Hydrogen.
4. The pressure inside the chamber is fixed at 10 torr, divided in 90% Argon and 10% Hydrogen, the temperature is kept stable at 1000 ℃ for 30 seconds.

5. The pressure inside the chamber is kept fixed at 10 torr, divided in 80% Argon, 10% Hydrogen and 10% Methane, the temperature is kept stable at 1000 ℃ for 120 seconds. This is the growth stage.
6. The pressure inside the chamber is fixed at 10 torr, divided in 90% Argon and 10% Hydrogen, the temperature is kept stable at 1000 ℃ for 30 seconds.
7. The slit heater is shut down and the temperature can freely decrease to 600 ℃, the gas flow into the chamber is now composed by 180 SCCM Argon, 10 SCCM Hydrogen and 10 SCCM Methane
8. From 600 ℃ to ambient temperature, the copper sample is cooled down exclusively by a gas flow of 200 SCCM Argon

In the cool down stage, the Methane injection grants a quicker temperature decrease with respect a gas flow of pure Argon. This behavior is due to the specific heat of methane (at constant pressure) which is $2470\frac{J}{Kg \cdot K}$, much higher than the Argon one (at constant pressure), which is only $520\frac{J}{Kg \cdot K}$.
At the end of this process the copper substrate is covered with a graphene monolayer on all his surface, it is important to mark (on the sample holder) (fig. 5.4) the side on which the graphene is grown, since it is not visible on the copper substrate.

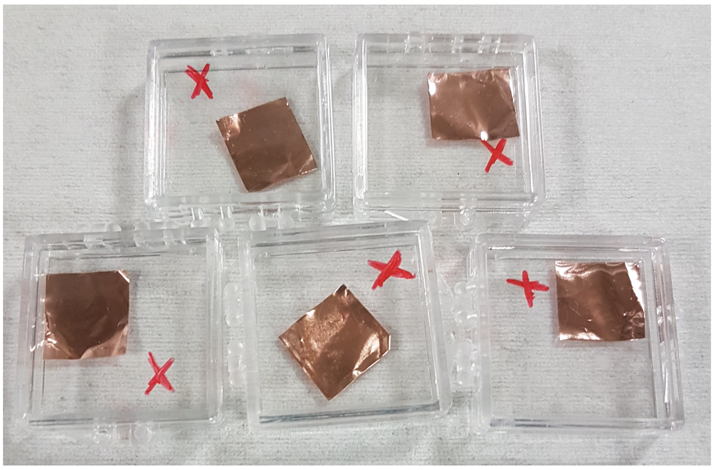

Figure 5.4: Copper samples housed into sample holders. It is noticeable that graphene, on this substrate, is not visible at naked eye.

5.2 Graphene transfer

In order to transfer the graphene onto a target substrate (fig. 5.5) there are a few steps and precautions to take into account.

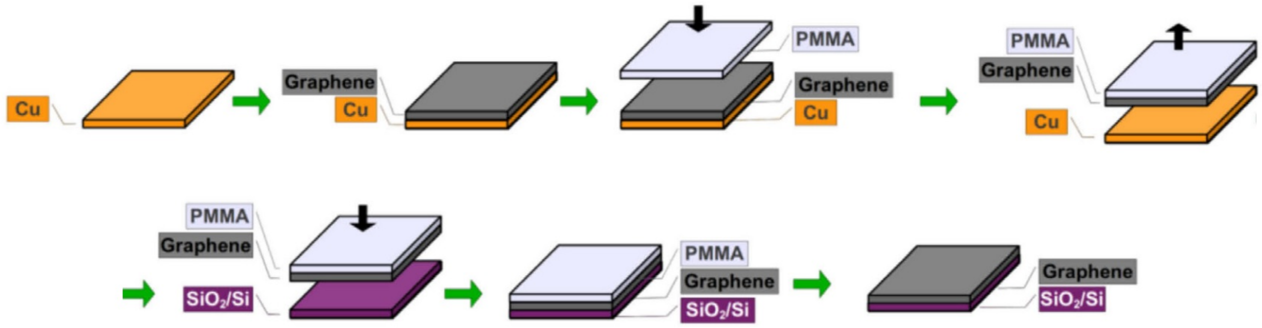

Figure 5.5: Graphene transfer process mediated by PMMA [17].

Since the graphene monolayer is thin and fragile, it needs a mechanical support that is able to assist the transfer process, avoiding its breakage and granting its positioning in the correct spot.
This kind of mechanical support could be granted by a thin layer of high diluted PMMA which is sufficiently resistant to avoid the breaking of the layer and sufficiently elastic to grant the complete adhesion of the graphene layer to the substrate. [17]
The PMMA solution is $4.5\%_{Wt}$ PMMA (*SIGMA ALDRICH, PMMA powder*) in Anisole (*SIGMA ALDRICH, anisole anhydrous 99,7%*) (fig. 5.6) .

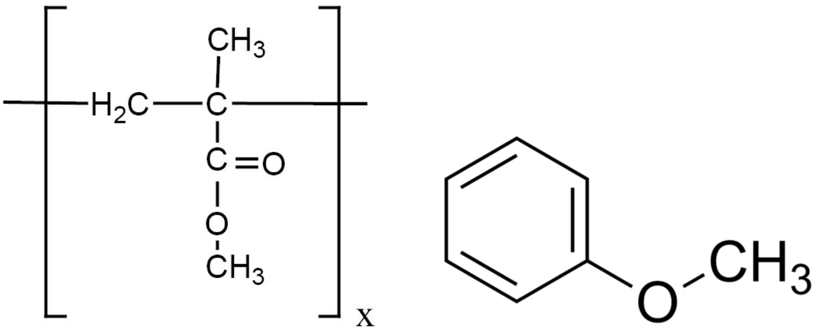

(a)

(b)

Figure 5.6: a) PMMA chemical formula, b) Anisole chemical formula

In order to create an homogeneous solution of PMMA in Anisole, a magnetical stirrer mixing was performed (fig. 5.7). Two hours should be enough to completely dissolve the PMMA in the solvent.

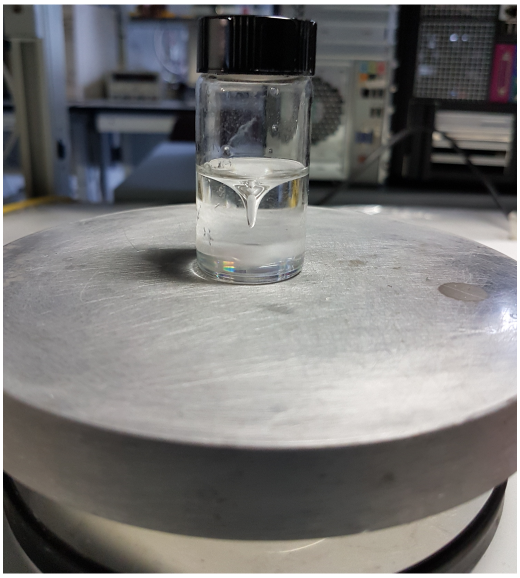

Figure 5.7: Solution preparation with the magnetic stirrer.

The graphene/copper samples needs now to be prepared for the PMMA coating. In order to ensure that the coating only occurs on the graphene side of the copper, it is mandatory to mask the edge of the sample (fig. 5.8). The masking operation is achievable with all kind of laboratory tape.

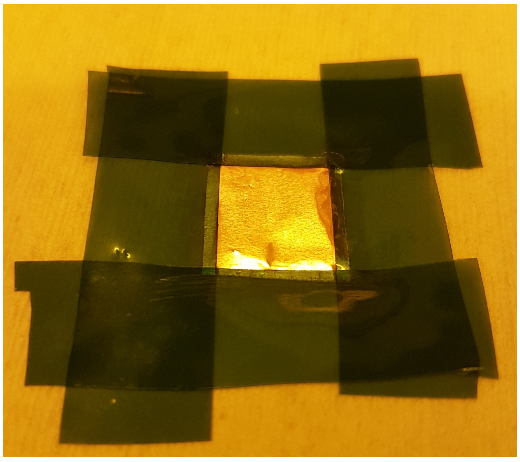

Figure 5.8: Sample masking with laboratory tape, the yellow light is due to the class 100 clean room illumination.

In order to perform the correct coating of the graphene/copper sample it is mandatory to use a spinner which can hold the sample and uniformly spread the PMMA solution on his surface exploiting the centripetal acceleration effect. The optimal settings are a plateau velocity of 2500 rpm for 90 seconds (fig 5.9a).
After the spin process it is necessary to cautiously remove the tape mask and anneal the sample on a hot plate at 80 °C for 15 minutes (fig. 5.9b), this step aims to completely evaporate the solvent (Anisole) and stick the PMMA to the graphene layer.

(a)

(b)

Figure 5.9: a) Spinner, the yellow light is due to the class 100 clean room illumination, b) Hot plate, the yellow light is due to the class 100 clean room illumination.

In order to transfer the graphene/PMMA sample onto the chosen substrate it is mandatory to remove the copper layer, this occur by etching.
The ferric chloride (*SIGMA ALDRICH, Ferric Chloride 97%*) is a copper etchant, the process is guided by the following chemical reaction in which the copper will be consumed from the sample to form the corresponding salt:

$$2FeCl4^{-} + Cu = 2Fe^{2+} + CuCl_4^{2-} + 4Cl^{-}$$

It is important to remark that the etchant should be used for many etching processes, this will simplify its disposal and allows a reduced usage of a potentially polluting substance.

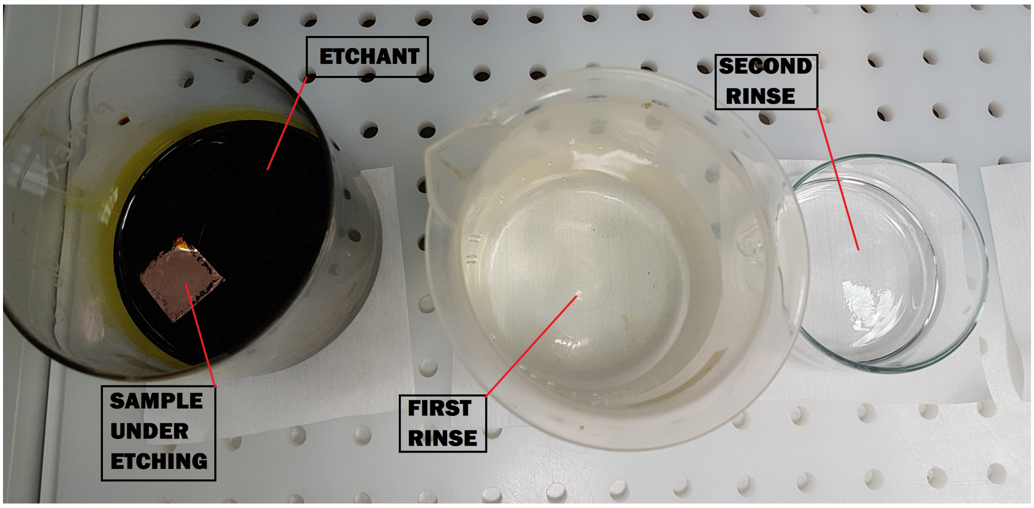

Figure 5.10: Etching procedure, general view.

When the etching procedure is complete, the copper is no longer attached to the graphene/PMMA layer; it is now fundamental to remove all the residual Ferric Chloride from his surface exploiting two rinse baths in deionized water. The diffusion effect will remove the etchant residual from the sample without the needs of a mechanical cleaning action, this will prevent the graphene layer from breaking (fig. 5.10) It is anyway possible to do more than two rinse steps, but it will only makes this procedure last longer without any concrete additional advantage (fig. 5.11).

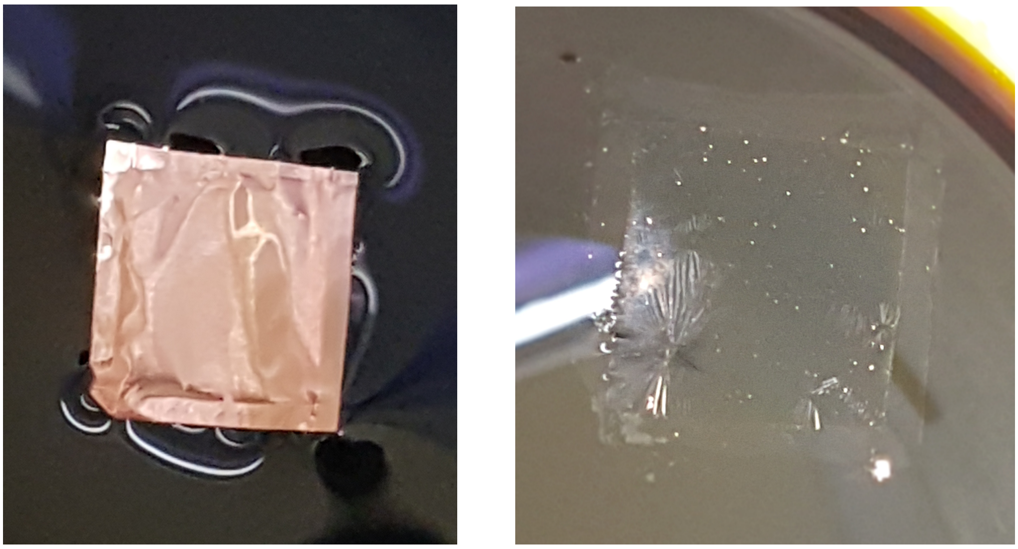

(a) (b)

Figure 5.11: a) Copper/graphene/PMMA sample in etching phase, b) PMMA/graphene sample at the end of the second rinse step.

The graphene/PMMA sample is ready to be transferred on the target substrate, for this experimentation it has been used a silicon substrate (without any presence of silicon oxide). Each silicon substrate is square shaped with edge equal to 20 mm, obtained from a 4 inch wafer cut using a circular diamond saw. Every silicon substrate was lightly engraved (on the back) to be easily physically divided in 16 squared subsection with edge equal to 5 mm (fig. 5.12).

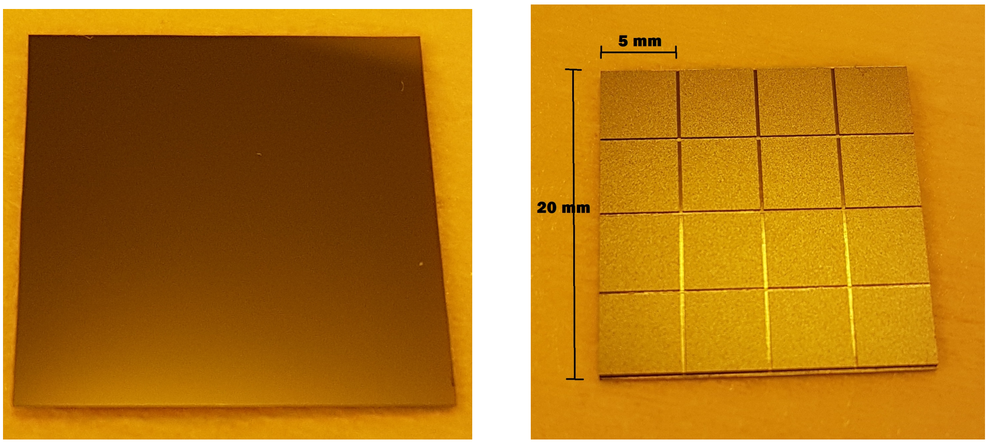

(a) (b)

Figure 5.12: Silicon substrate. The yellow light is due to the class 100 clean room illumination. a) front view, b) back view.

Each silicon sample must be cleaned with Acetone (*SIGMA ALDRICH, Acetone 99,5%*) and Isopropanol (*SIGMA ALDRICH, Isopropanol 99.7%*) in order to remove all the impurities that may have deposited on its surface and restore its wettability.

The graphene/PMMA sample must be caught from the rinse bath and dried on the silicon substrate using a nitrogen gun, the drying action will remove the bigger part of residual water and will anchor the graphene layer to the substrate. It is now useful to continue the drying process on an hot plate, this procedure is divided in two stages in order to grant a gradual heating and to not damage the Graphene/PMMA layer: on first phase, the plate is heated up to 80 ℃ for 5 minutes, this will remove the bigger part of water remained from the nitrogen drying. On second phase the plate is heated up to 130 ℃ in order to complete the drying process without any water residue.

Once completely dried, the PMMA protective layer needs to be removed in order to expose the underlying graphene. This could done in an Anisole bath, lasting longer than twenty minutes, which is able to dissolve the PMMA layer leaving minimal traces on the graphene layer. It is fundamental to understand that the PMMA layer will always leave some residue and it is not possible to obtain a completely clean substrate using PMMA as a supportive layer.

5.2.1 Vacuum drying

After the graphene/supporting-layer transfer, the sample could be dried in a vacuum chamber instead of an hot plate. The vacuum will contribute to promote the adhesion between graphene and the substrate meanwhile all the residual water is removed. This procedure does not offer any particular quality advantage with respect the main procedure, so is possible to assert that it is an alternative way, able to grant the same qualitative results as the thermal drying.
Relying on the chamber dimension, and differently from the hot plate, the vacuum drying may be used to dry more than one sample at the time, increasing the saving of time and energy (fig. 5.13).

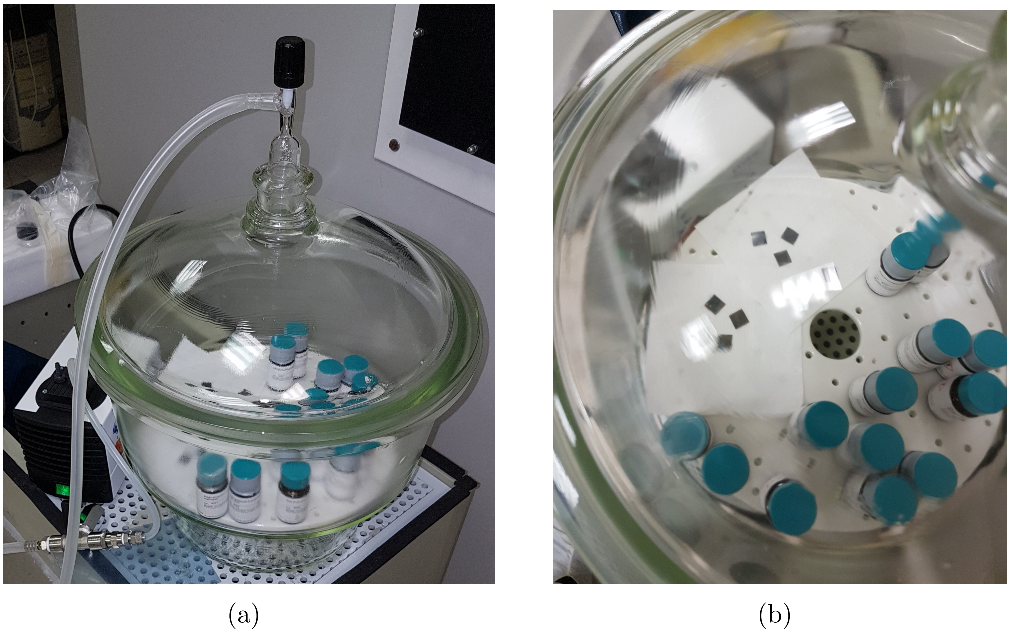
(a) (b)

Figure 5.13: Vacuum chamber used to dry the samples. a) front view, b) top view.

5.2.2 Supporting layer removal by sonication

After the graphene/supporting-layer drying, the supporting layer can be removed in a solvent bath with the addition of a sonication process instead of a normal solvent bath. This procedure remove more effectively the supporting-layer leaving a lot less residual, but it tends to damage the underlying graphene layer, compromising its quality. The use of this technique could be effective only to remove a particularly strong supportive layer.

5.2.3 Shellac as supporting layer

The use of PMMA as supporting layer is the most common way to perform a graphene transfer, this technique have the only physical drawback in the residues left on the graphene surface that, according to the use for which it is intended, may require different degrees of cleanliness. Another fact that is important to take into account, is that the PMMA is an expensive and absolutely not eco-friendly material and even less when paired with anisole. A possible solution to this problem is to use Shellac instead of PMMA.

Shellac is a resin secreted by the female lac bug, on trees in the forests of India and Thailand. It is processed and sold as dry flakes and dissolved in Ethanol to make liquid shellac, which is usually used as a brush-on colorant, food glaze and wood finish. Shellac works as a tough natural primer, sanding sealant, tannin-blocker, odour-blocker. Shellac was once used in electrical applications as it possesses good insulation qualities. Shellac naturally contains a small amount of wax (from 3% to 5% by volume), which comes from the lac bug. In this specific usage the wax is removed (the resulting product is called "dewaxed shellac") (fig. 5.14).
Shellac is a natural bioadhesive polymer and is chemically similar to synthetic polymers, so can be considered a "natural form" of plastic classifiable as thermoplastic. This material is soluble in alkaline solutions such as Ammonia, Sodium borate, Sodium carbonate, Sodium Hydroxide, and also in various organic solvents.
When dissolved in Ethanol, shellac shows a coating of good durability and hardness, which qualifies it as a good replacement for PMMA. Furthermore, Shellac is UV-resistant, and does not darken as it ages, opening the possibility to coat graphene to prevent its oxidation.
In the process of graphene transfer, Shellac can substitute PMMA with some substantial differences in the "transfer operative procedure":


Figure 5.14: Dewaxed shellac

- Shellac (*SINOPIA, dewaxed Shellac*) must be diluted at $5\%_{vol}$ in Ethanol (SIGMA ALDRICH, Ethanol 99,8%) in order to obtain an adequate coating of the graphene surface.
- The spinning process must be reduced in the plateau velocity, now set to 900 rpm for 90 seconds.
- Due to the termoplastic nature of Shellac, the annealing process must be performed at a temperature of 35 ℃ for 15 minutes.
- The hot plate drying procedure must be performed at 35 ℃ for 20 minutes.

- Shellac removal must be performed by an Ethanol bath lasting longer than twenty minutes.

This procedure allow to produce graphene of comparable quality to the PMMA one. The difference between the two methods sits in the cost (dewaxed flaked Shellac is up to 900% cheaper than powdered PMMA) and in the environmental impact of the processing residues, way less dangerous with the Shellac transfer.

Chapter 6

Graphene Characterization

6.1 Raman Characterization

In this section will be presented the comparison between the Raman spectra obtained from the four graphene growing recipes discussed in chapter 4.1.
Initially it is useful to notice that the Raman equipment cannot filter out the Copper spectrum from the characterization results. Therefore the output spectrum will be the sum of the Copper one (treated like an unwanted noise) plus the graphene one. This condition does not allow to obtain any information regarding the quality of the graphene layer (fig. 6.1 - 6.2 - 6.3).

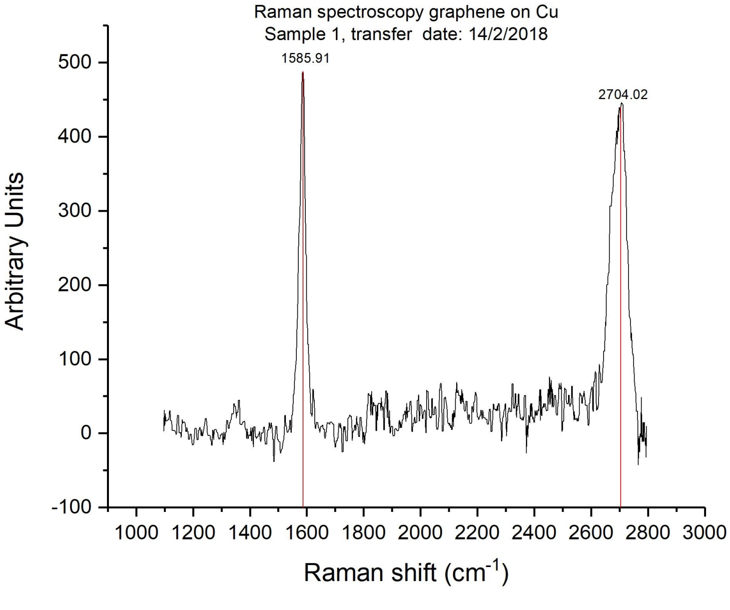

Figure 6.1: Laboratory sample 1 (**Recipe 1**, ref. chapter 5), Raman spectra, graphene on copper.

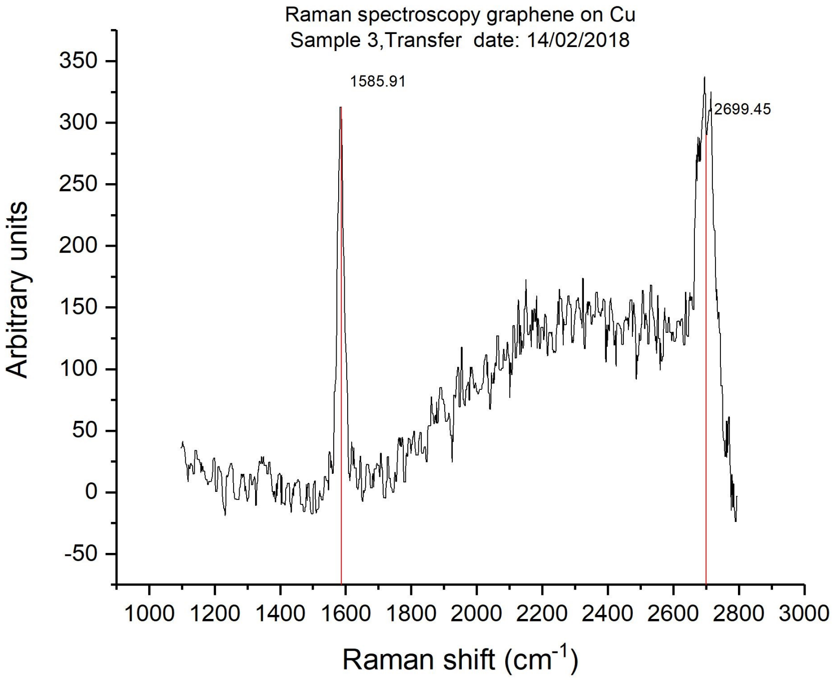

Figure 6.2: Laboratory sample 3 (**Recipe 3**, ref. chapter 5), Raman spectra, graphene on copper.

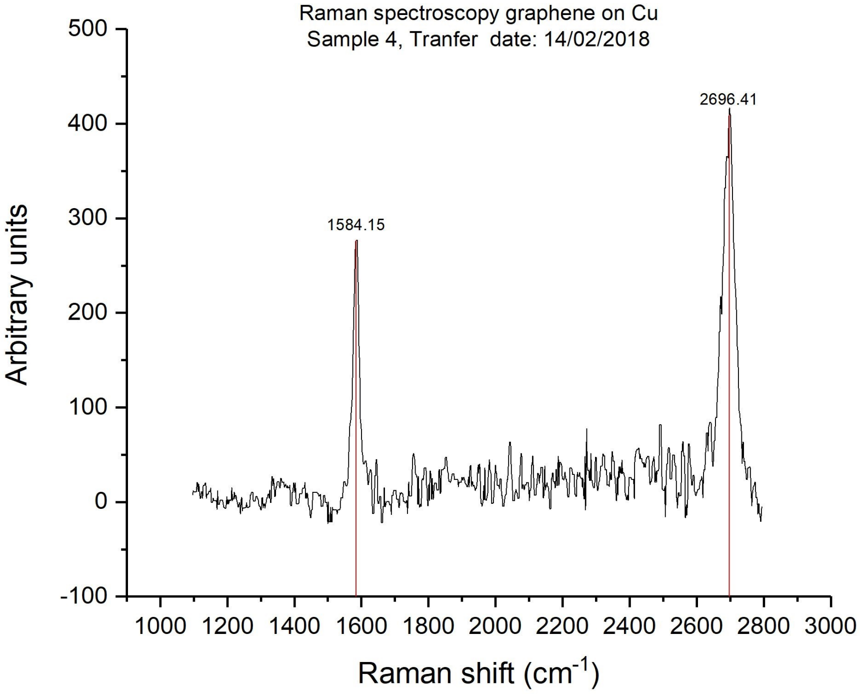

Figure 6.3: Laboratory sample 4 (**Recipe 4**, ref. chapter 5), Raman spectra, graphene on copper.

Looking at the spectra of the four samples of graphene on Si substrate (fig. 6.4 - 6.5 - 6.6 - 6.7), it is possible to notice that, according to literature (comparison on fig. 6.9), all the samples show an high quality and a monolayer behavior. At $1350 cm^{-1}$ and $1440 cm^{-1}$ is located a two tips peak which is a residual of the silicon substrate spectrum. When the graphene layer is defective, damaged or discontinuous, the silicon substrate noise peaks is sharper; in case of well constructed graphene, the silicon peak is larger and wider (fig. 6.9) [13, 14].
At $1584 cm^{-1}$ lays the G-band peak, according to literature this is an index of the defectiveness of the graphene layer: the more the peak is sharper, the less defective the graphene is. The sample number one (recipe 1 ref. chapter 5) results to be the most defective one (comparison on fig. 6.8a), this characteristic is highlighted by the wider base of the G-peak. Consequently the less defective sample results to be the number four (fig. 6.7, recipe 4 ref. chapter 5). Moreover the position of the G-peak offers information about the quantity of layers of the graphene sample. When the center of the peak is located at $1582 cm^{-1}$ the sample results to be monolayer, contrarily to when it is located at $1560 cm^{-1}$ which is the characteristic Raman shift of the Graphite. The number of layers of the sample increase linearly with the increasing of the peak center Raman shift between the two mentioned values (fig. 6.10a). Comparing all the samples with the literature highlights that all of them show a monolayer behavior but the best in terms of defectiveness results to be the number four (fig. 6.10, recipe 4 ref. chapter 5) [13, 14].
Precisely at $2321.5 cm^{-1}$ there is a peak which is an artifact generated by the Raman equipment. At $2690 cm^{-1}$ sits the 2D-band peak which, according to literature, is another discrimination index between monolayer graphene and multilayer graphene. An high and sharp peak with its center located at $2690 cm^{-1}$ is index of a monolayer sample. The presence of the $2D_1$-peak as a left enlargement of the 2D-peak base, and its center shift to $2725 cm^{-1}$ is contrarily index of a graphite sample. The number of layers of the sample increase linearly with the shape of the peak base, and with the increasing of the peak center Raman shift between the two mentioned values (fig. 6.11a - 6.11b). All of the four samples (recipes ref. chapter 5) have monolayer characteristic (fig. 6.8b) but the best shaped 2D-peak belongs to the sample number four (fig. 6.7 - 6.11, recipe 4 ref. chapter 5) [13, 14]. Taking into account what has been previously highlighted regarding the graphene Raman spectrum, it is now possible to assert that the sample number four (fig. 6.7 - 6.9, recipe 4 ref. chapter 5) is the best one, both for his monolayer characteristic and his reduced quantity of defects. These results has been produced with the PMMA transfer technique. Nevertheless it is important to remark that the transfer technique, whatever it is, cannot influence the samples number of layers because it take place after the complete growth of the graphene. The main purpose of each transfer technique is to move the graphene layer from one substrate to another minimizing the mechanical stresses that are responsible of induced defects [17].

	Growth time	Cooling atmpsphere
Sample 1	300 s	Argon
Sample 2	300 s	Methane
Sample 3	120 s	Argon
Sample 4	120 s	Methane

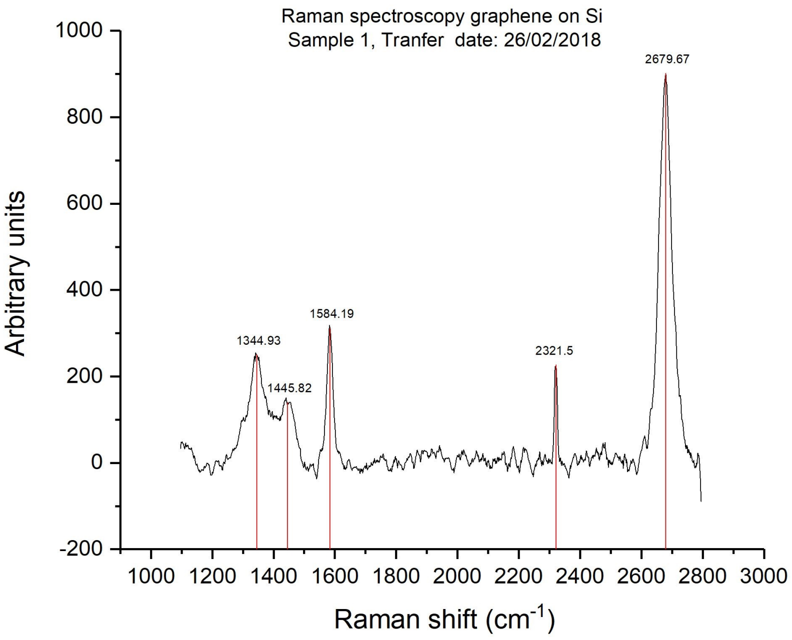

Figure 6.4: Laboratory sample 1 (**Recipe 1**, ref. chapter 5), Raman spectrum, graphene on silicon oxide.

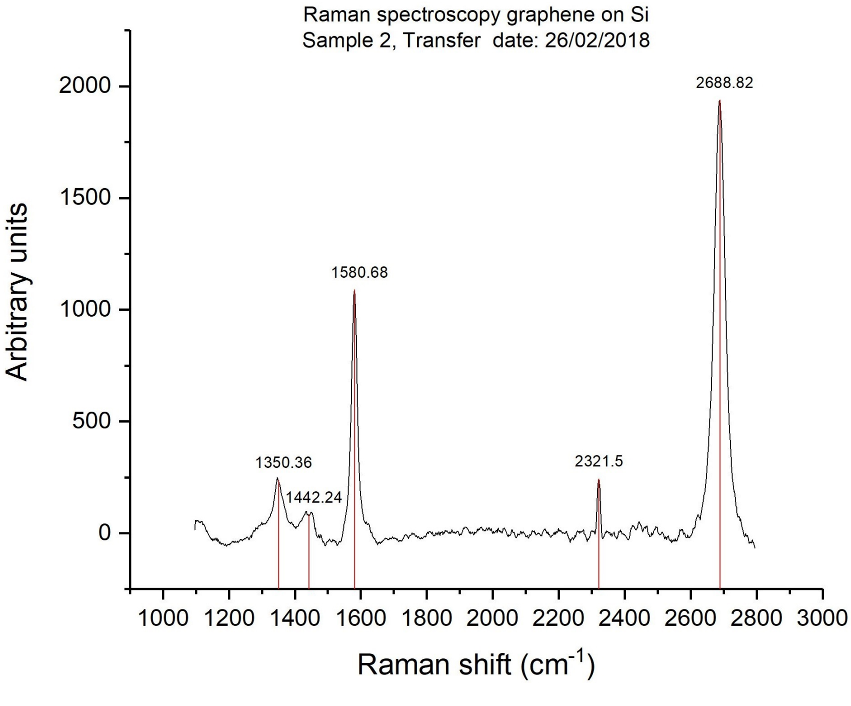

Figure 6.5: Laboratory sample 2 (**Recipe 2**, ref. chapter 5), Raman spectra, graphene on silicon oxide.

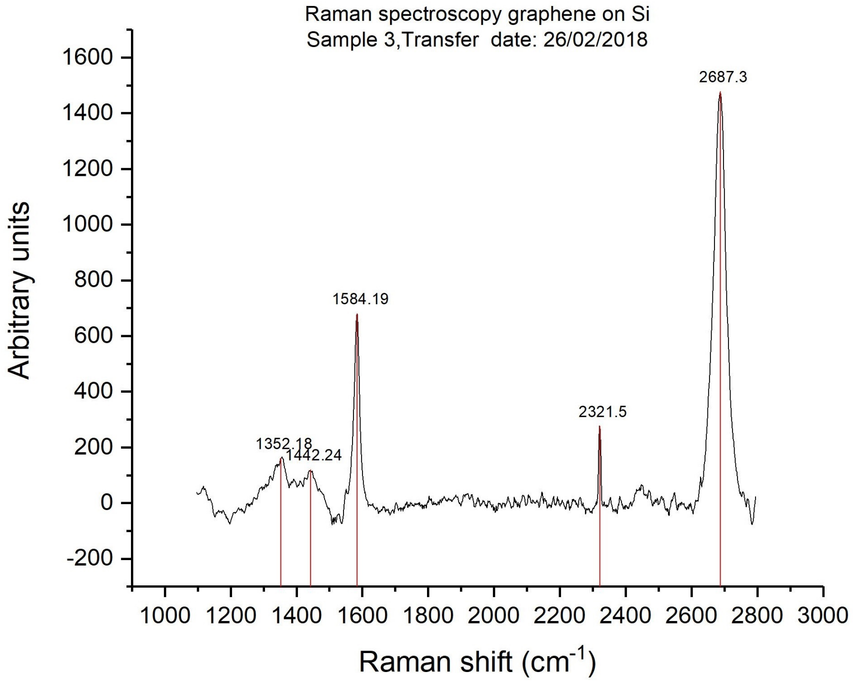

Figure 6.6: Laboratory sample 3 (**Recipe 3**, ref. chapter 5), Raman spectra, graphene on silicon oxide.

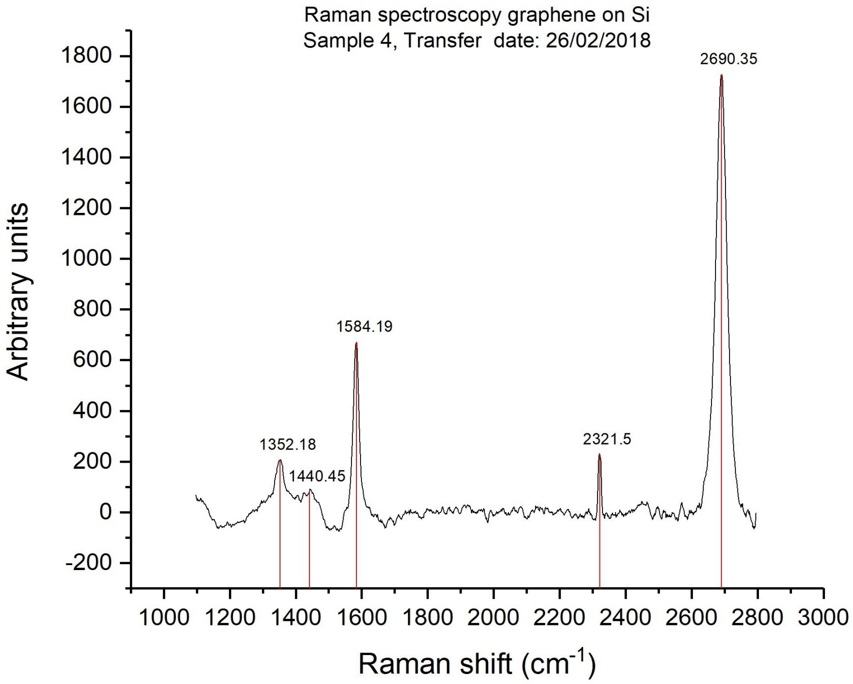

Figure 6.7: Laboratory sample 4 (**Recipe 4**, ref. chapter 5), Raman spectra, graphene on silicon oxide.

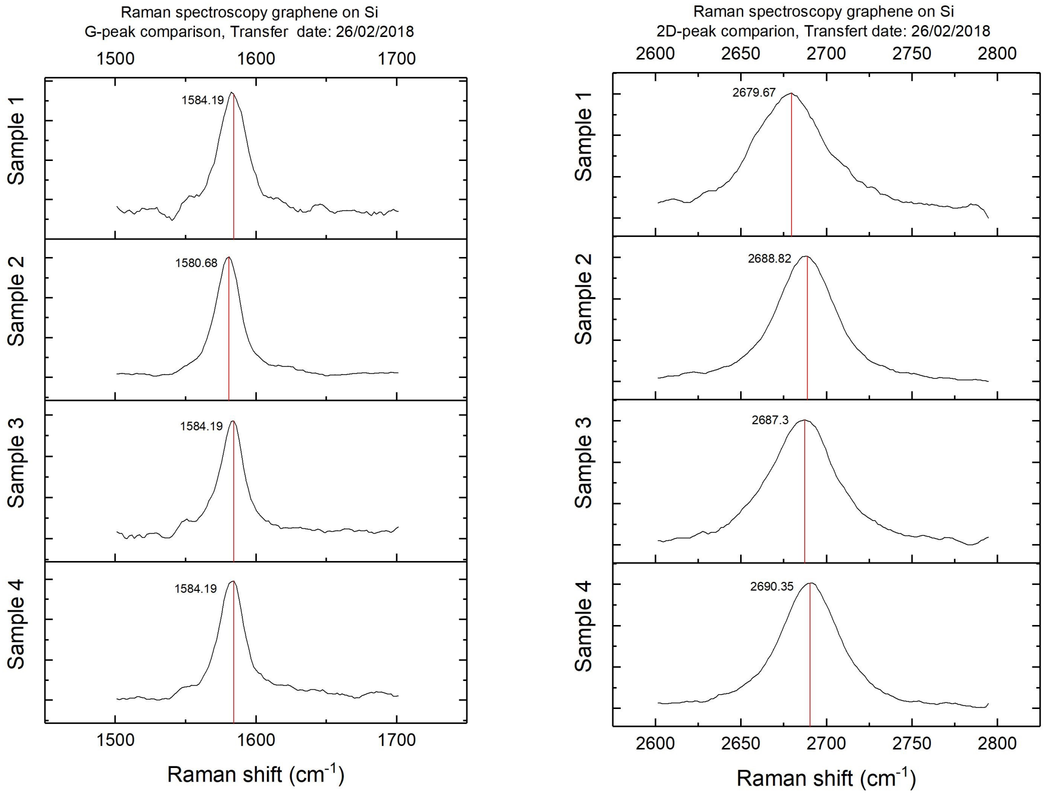

(a) (b)

Figure 6.8: a) Laboratory samples G-peak comparison, b) Laboratory samples 2D-peak comparison

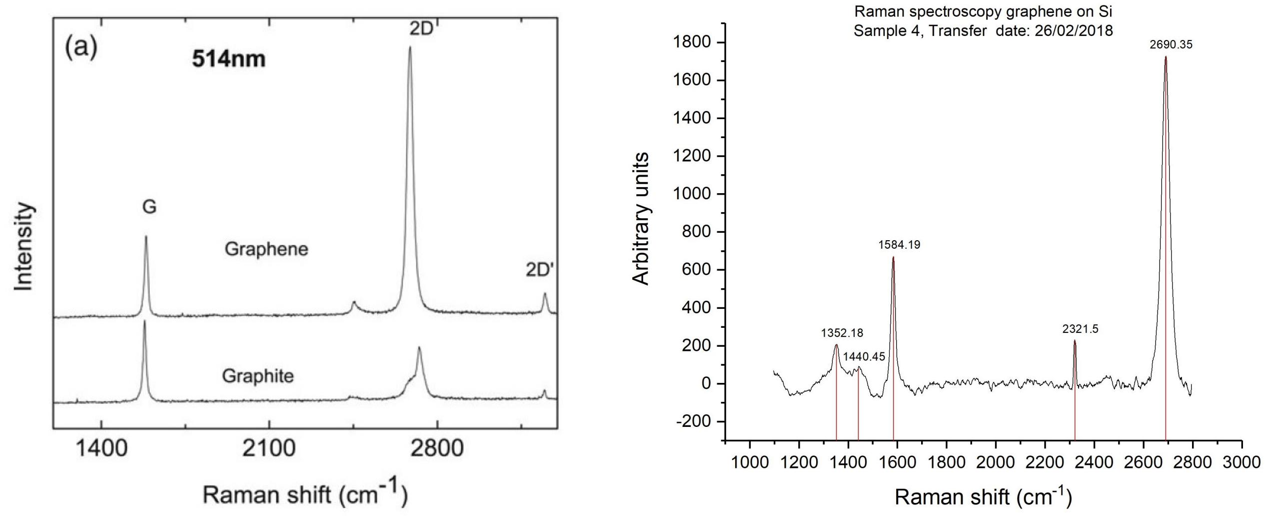

(a) (b)

Figure 6.9: a) Raman spectra matching between graphene and graphite (substrate SiO_2) [14] b) laboratory sample 4 (substrate Si, recipe ref. chapter 5),

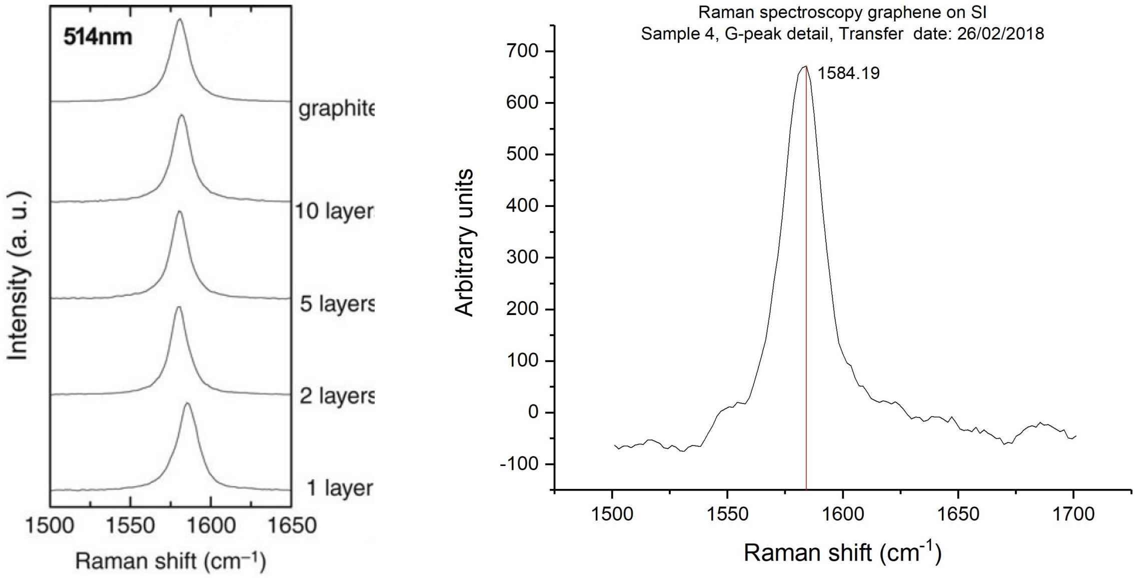

(a) (b)

Figure 6.10: a) Raman spectra G-peak matching between graphene (located at $1584cm^{-1}$ Raman shift) and graphite [14], b) laboratory sample 4 (recipe ref. chapter 5).

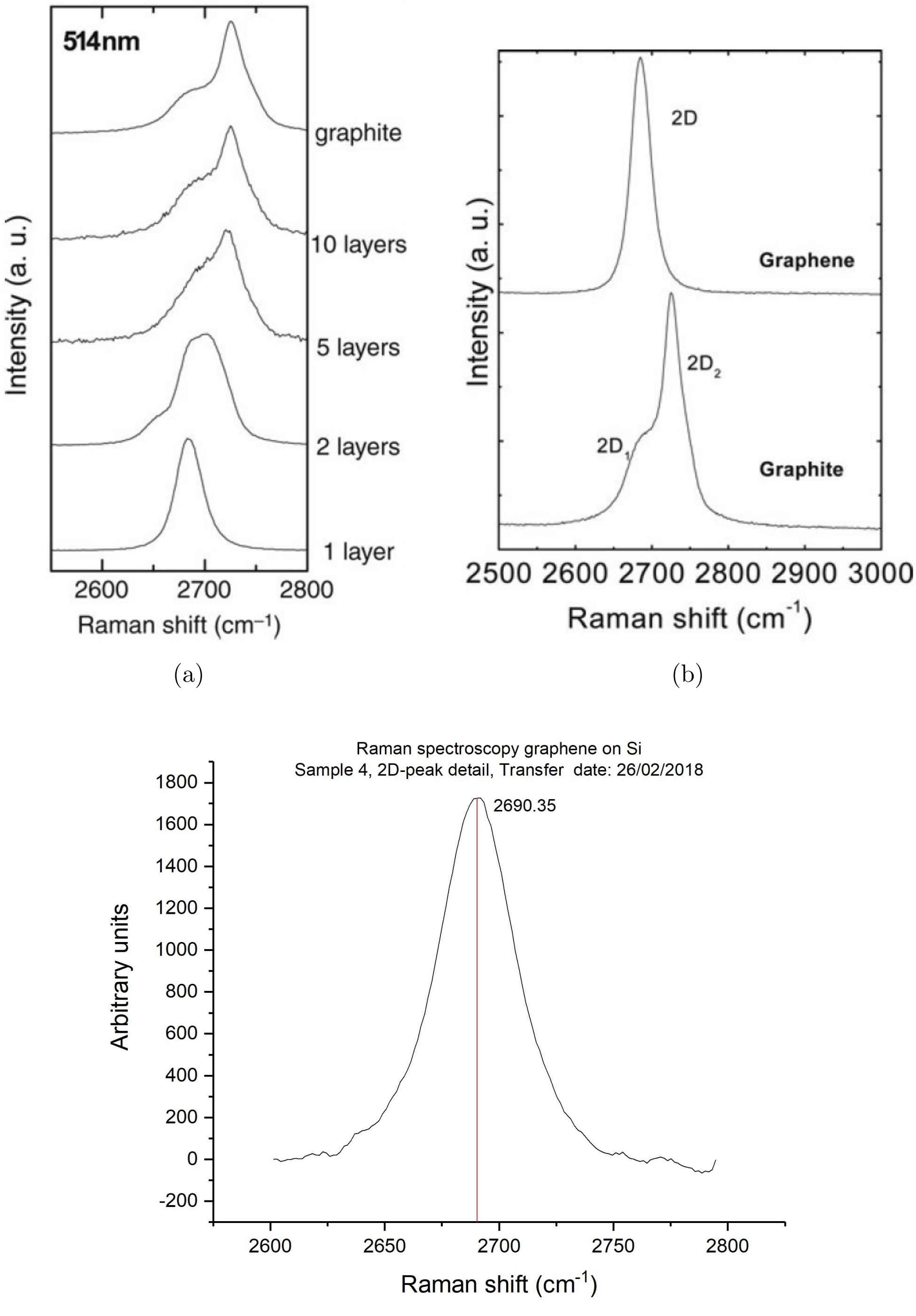

(a)

(b)

(c)

Figure 6.11: a,b) Raman spectra 2D-peak matching between graphene (located at $2685cm^{-1}$ Raman shift) and graphite [14], c) laboratory sample 4 (recipe ref. chapter 5).

The Raman characterization of a graphene sample, grown using the best quality growing recipe ”number 4” (sample 4 recipe ref. chapter 5) and transferred with shellac shows this material as suitable for the role of supporting layer. The graphene quality is not afflicted by the different material with respect to the PMMA one (fig. 6.12), the main drawback using Shellac sits in the removal procedure. It is mandatory to absolutely not use any sonication procedure trying to speed up the removal time or to decrease the quantity of residue, otherwise the underlying graphene layer will be damaged or partially removed in the process.

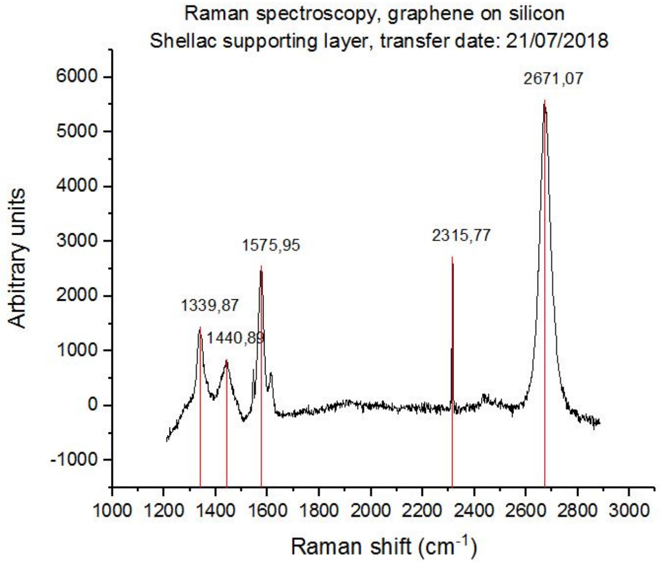

(a)

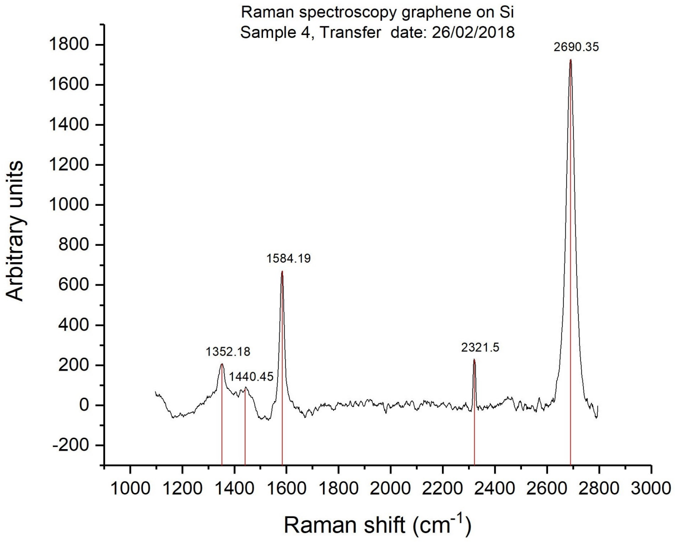

(b)

Figure 6.12: a) Raman spectrum of a Shellac mediated transfer graphene layer, b) Raman spectrum laboratory sample 4 (substrate Si) PMMA transfer

6.2 Field Emission Scanning Electron Microscopy - FESEM characterization

The FESEM characterization allows to identify, in a gray scaled image, the edges of a graphene monolayer, which can be identified from his peculiar planar surface without any wrinkle (fig. 6.13).
If the graphene layer suffer some ruffles (fig. 6.14), as a consequence of an incorrect sample manipulation during the transfer process, it is possible to identify the defective zone by simply looking at its peculiar shape. With this characterization technique it is also possible to evaluate if the supporting layer has been removed and, eventually, the quantity and the distribution of residues (fig. 6.14b).
Magnifying the image 6.14c, it is possible to notice some "white dots" which are residual from the copper etching procedure, this "residue" cannot be removed or avoided in any way but changing the graphene production technique.

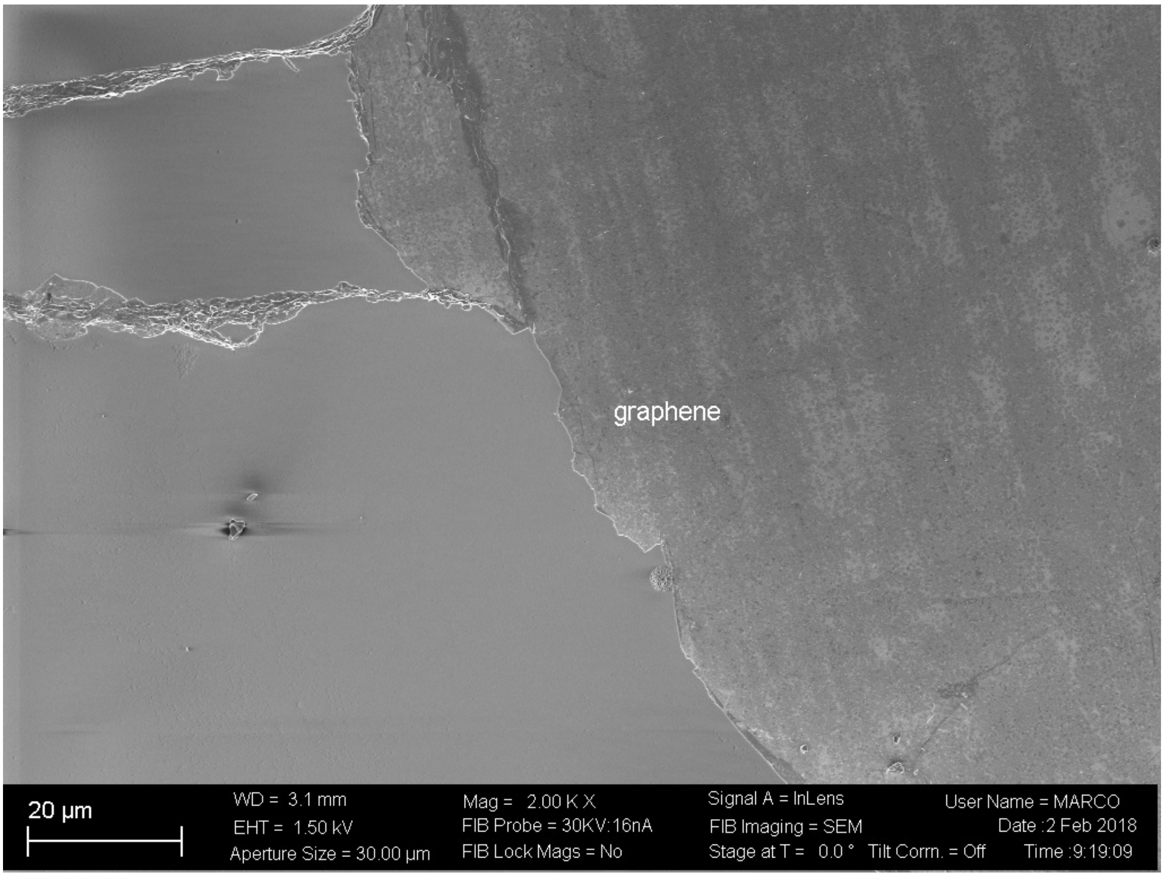

Figure 6.13: Laboratory FESEM image: in this image is possible to appreciate a graphene layer which is identifiable by its edge

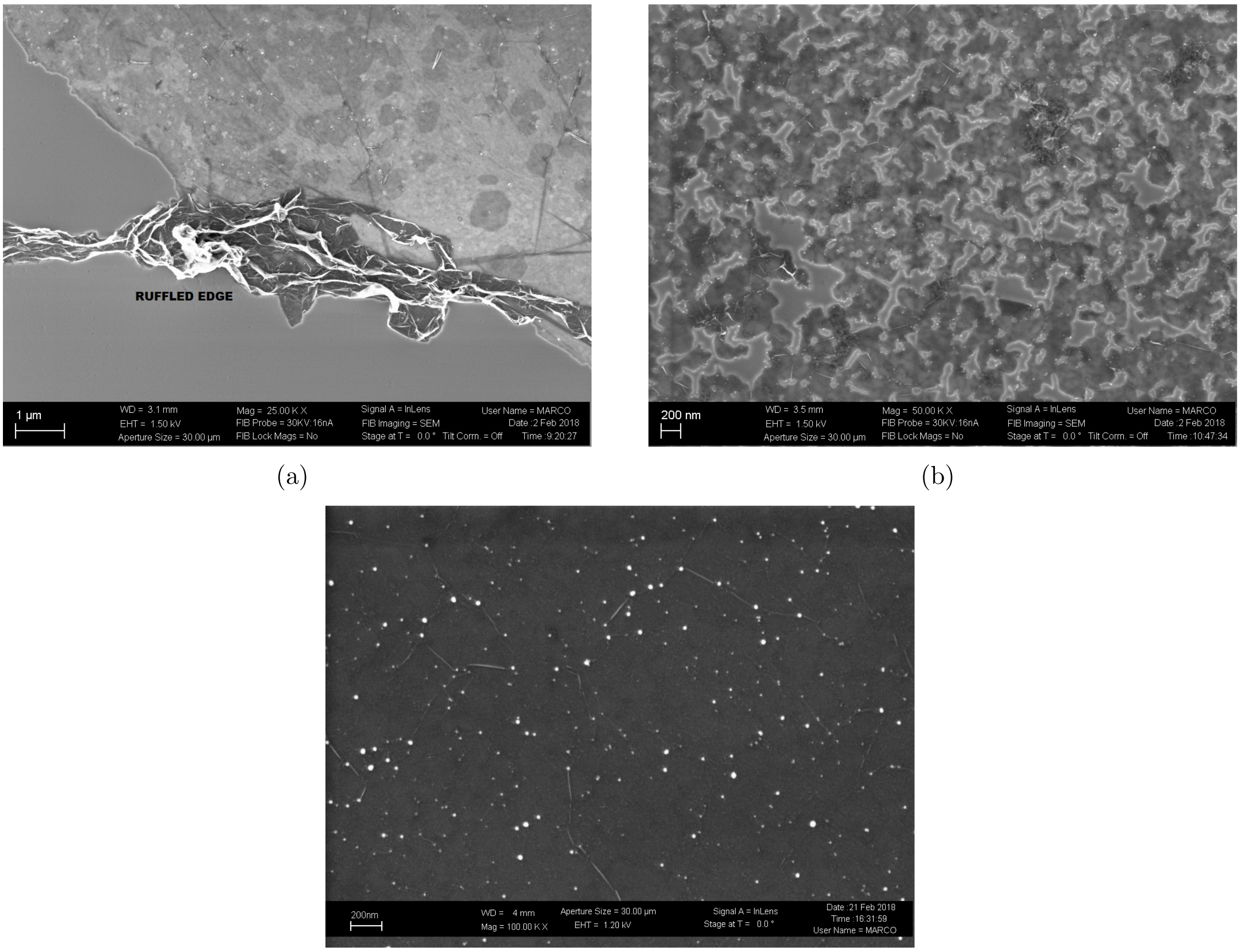

(a) (b)

(c)

Figure 6.14: Laboratory FESEM images. a) Graphene ruffled edge, b) Incorrect PMMA removal from the graphene surface (darker spots in relief), c) Copper residue on graphene surface (white dots)

6.3 X-Ray Photoelectron Spectroscopy - XPS characterization

As mentioned before (Chapter 3.2.3), The XPS characterization give important information regarding the elemental composition of the analyzed sample surface.
The higher percentage of Carbon (around 65%) found in the samples 2 and 4 (fig. 6.16 - 6.18, recipes 2 and 4 ref. chapter 5), compared with the other two samples, is clue that the cooling stage in Methane atmosphere, imposed to these samples, guarantees a more uniform and extended graphene coverage. Furthermore the growing stage imposed to 120 seconds, peculiar to samples 3 and 4 (fig. 6.15 - 6.17, recipes 3 and 4 ref. chapter 5), guarantees a lesser Oxygen percentage (18% against 22%) with respect the samples 1 and 2 (which have a growing stage of 300 seconds, recipe 1 and 2 ref. chapter 5), suggesting a reduced oxidation of the graphene layer that coincides with its minor defectiveness.
This characterization is a further demonstration of the superior quality of the sample number 4 (**Recipe 4**, ref. chapter 5).

	Growth time	Cooling atmpsphere
Sample 1	300 s	Argon
Sample 2	300 s	Methane
Sample 3	120 s	Argon
Sample 4	120 s	Methane

Samples summary table (ref. chapter 5)

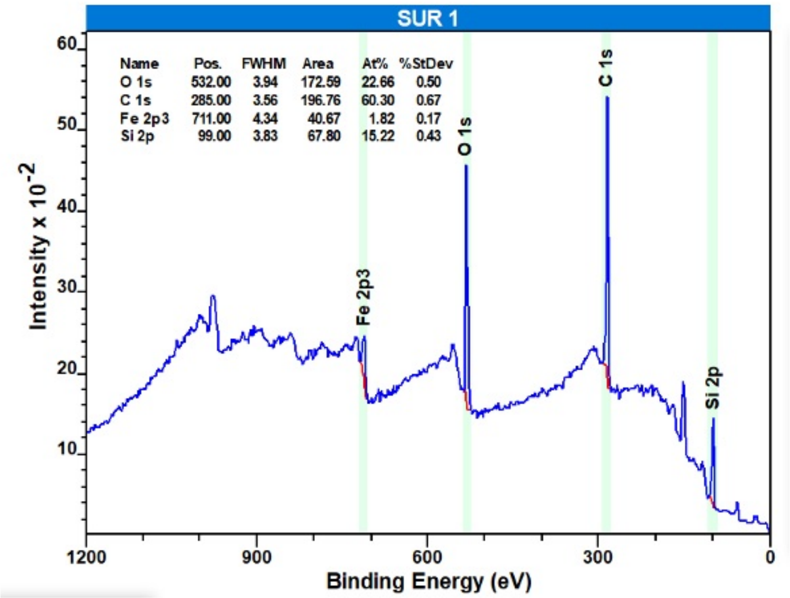

Name	Pos.	FWHM	Area	At%	%StDev
O 1s	532.00	3.94	172.59	22.66	0.50
C 1s	285.00	3.56	196.76	60.30	0.67
Fe 2p3	711.00	4.34	40.67	1.82	0.17
Si 2p	99.00	3.83	67.80	15.22	0.43

Figure 6.15: XPS characterization of the laboratory sample 1 (**Recipe 1**, ref. chapter 5)

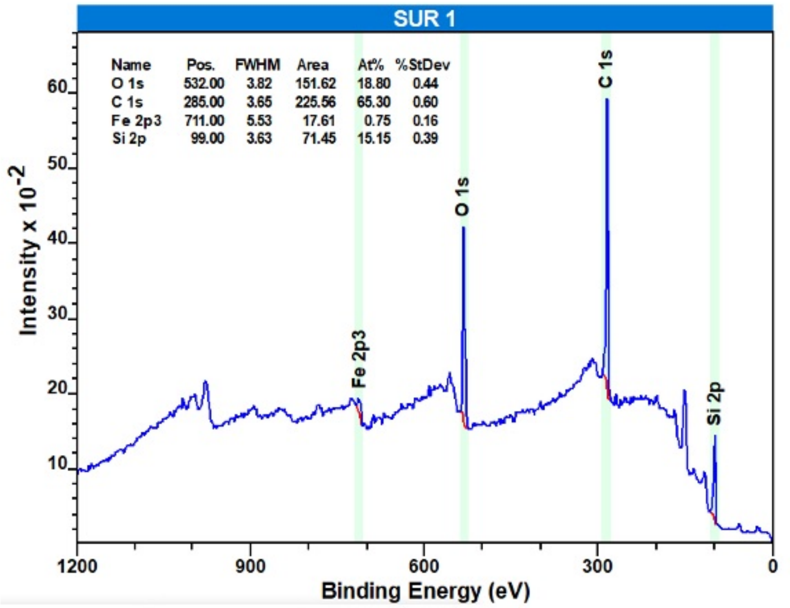

Name	Pos.	FWHM	Area	At%	%StDev
O 1s	532.00	3.82	151.62	18.80	0.44
C 1s	285.00	3.65	225.56	65.30	0.60
Fe 2p3	711.00	5.53	17.61	0.75	0.16
Si 2p	99.00	3.63	71.45	15.15	0.39

Figure 6.16: XPS charactherization of the laboratory sample 2 (**Recipe 2**, ref. chapter 5)

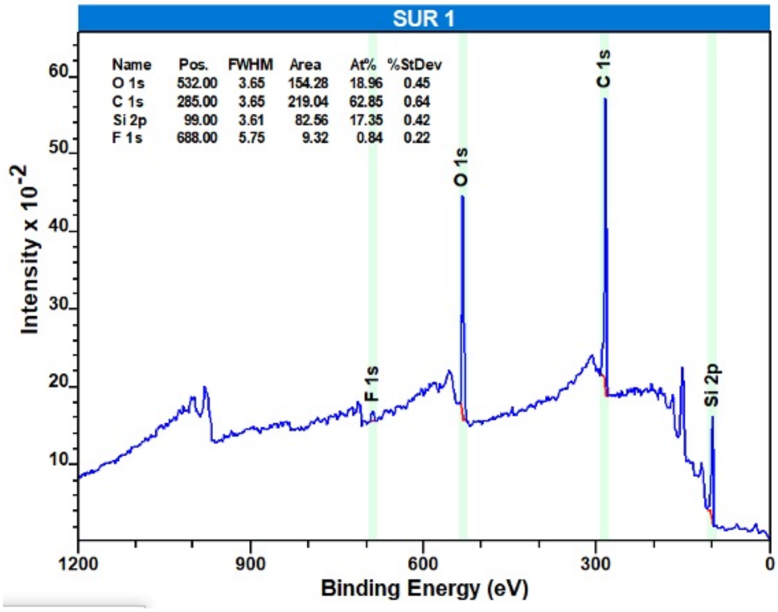

Name	Pos.	FWHM	Area	At%	%StDev
O 1s	532.00	3.65	154.28	18.96	0.45
C 1s	285.00	3.65	219.04	62.85	0.64
Si 2p	99.00	3.61	82.56	17.35	0.42
F 1s	688.00	5.75	9.32	0.84	0.22

Figure 6.17: XPS charactherization of the laboratory sample 3 (**Recipe 3**, ref. chapter 5)

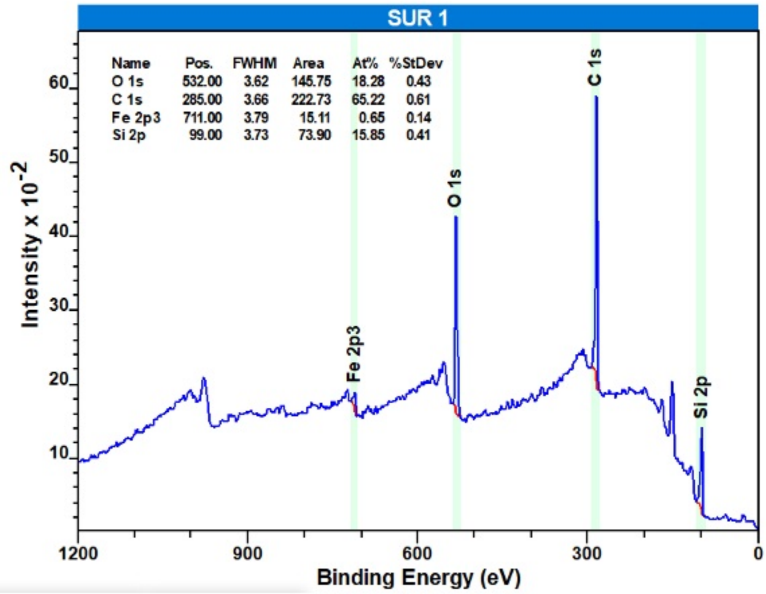

Name	Pos.	FWHM	Area	At%	%StDev
O 1s	532.00	3.62	145.75	18.28	0.43
C 1s	285.00	3.66	222.73	65.22	0.61
Fe 2p3	711.00	3.79	15.11	0.65	0.14
Si 2p	99.00	3.73	73.90	15.85	0.41

Figure 6.18: XPS characterization of the laboratory sample 4 (**Recipe 4**, ref. chapter 5)

Chapter 7

Electrolyte gated GFET - A practical application

A good application in which it is possible to test the quality of the produced graphene is an Electrolyte gated GFET. Both of the transfer techniques (PMMA and shellac) has been used in order to obtain an electrical characterization of the produced graphene. At the end of the process flow, an array of ten transistor was produced.

7.1 Electrolyte gated GFET production process flow

Starting from a rectangular oxidized silicon substrate ($24mm$ wide, $15mm$ tall), using an Electron-beam Physical Vapor Deposition process, a layer of titanium $10nm$ thick, which act as adhesion promoter, has been deposited over the Silicon Oxide surface. Immediately afterwards a gold layer $100nm$ thick was deposited, the adhesion of this layer is promoted by the presence of Titanium (fig. 7.1).

Figure 7.1: Electrolyte gated GFET: Titanium and Gold EBPVD

A photo lithographic process is now necessary in order to selectively remove a portion of Titanium/Gold, creating the channel housing. The photo-resist Az 1518 has been used in order to pattern the sample gold surface (fig. 7.2).

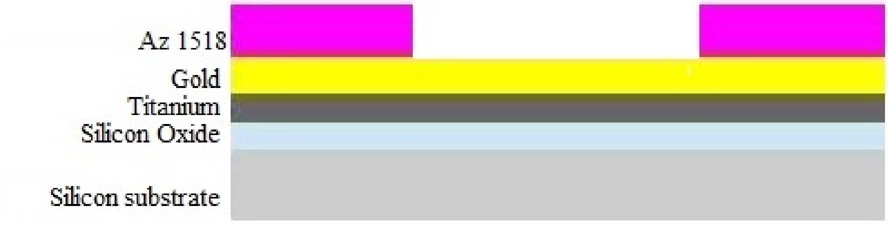

Figure 7.2: Electrolite gated GFET: First Az 1518 photo lithografic step

In order to create the channel housing, it is necessary to etch the uncovered Gold layer and then the sequentially exposed Titanium layer (fig. 7.3). To perform the gold etching, Nitrohydrochloric acid has been used, once this mixture of Nitric acid and Hydrochloric acid enter in contact with Gold, this chemical reaction occurs:

$$Au + 3HNO_3 + 4HCL \longleftrightarrow [AuCl_4]^- + 3NO_2 + [H_3O]^+ + 2H_2O$$

To perform the Titanium etching, a mixture of Hydrofluoric acid and Nitric acid has been used. Although Hydrofluoric acid is a good Titanium etchant by himself, is convenient to add some Nitric Acid in order to block the production of Hydrogen gas (which is flammable and explosive) and speed up the etching process. The chemical reaction that occurs is:

$$Ti + 6HF + 4HNO_3 \rightarrow H_2TiF_6 + 4NO_{2_{gas}} + 4H_2O$$

As it is possible to notice, the Hydrogen production is eliminated.

Figure 7.3: Electrolite gated GFET: Gold and Titanium etching

The channel is now ready to house the graphene layer which is transfered with the procedure previously discussed (Chapter 4.2). In order to protect the graphene , is convenient to deposit a copper layer $50nm$ thick (EBPVD) (fig. 7.4).

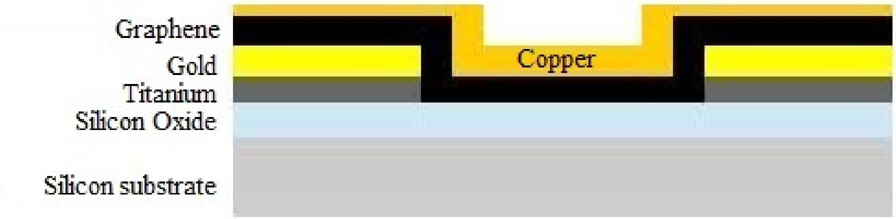

Figure 7.4: Electrolite gated GFET: graphene transfer and copper EBPVD

The excess of copper and graphene which sits on the gold contact must be removed. Therfore an oxygen-plasma etching technique has been used to reach this purpose, the channel area has been protected from the etching with a thick layer of Photo-resist Az 1518 (fig. 7.5 - 7.6 - 7.7).

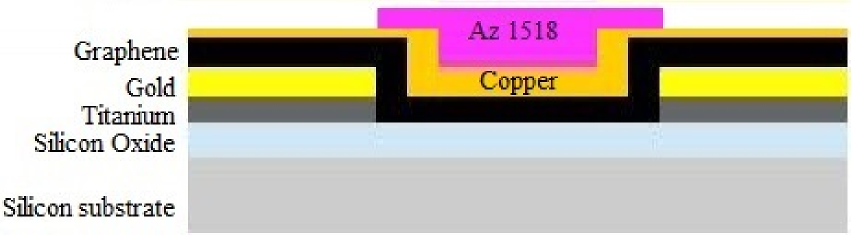

Figure 7.5: Electrolite gated GFET: Channel masking with Az 1518

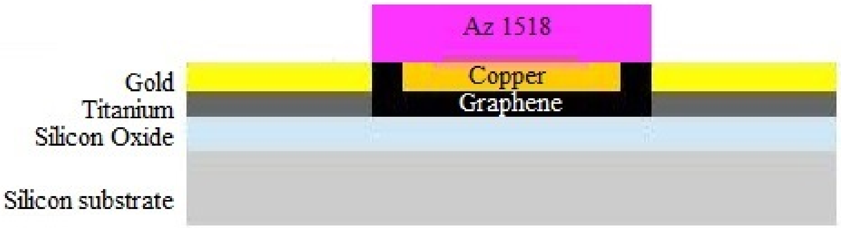

Figure 7.6: Electrolite gated GFET: Oxigen-plasma etching of excess Copper and graphene

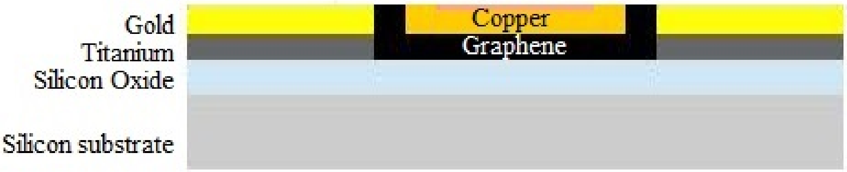

Figure 7.7: Electrolite gated GFET: Az 1518 masking layer removal

The whole structure needs to be passivated, for this purpose it has been used a patterned layer of Alumina deposited with the Electron-beam Physical Deposition technique (fig. 7.8 - 7.9). The Alumina (Aluminum oxide) is a chemical compound of Oxygen and Aluminum, with the chemical formula Al_2O_3. It is an electrical insulator with a thermal conductivity of 30 $Wm^{-1}K^{-1}$. In order to selectively lift off the Alumina layer, it has been used a patterned layer of Az 5214 photo-resist.

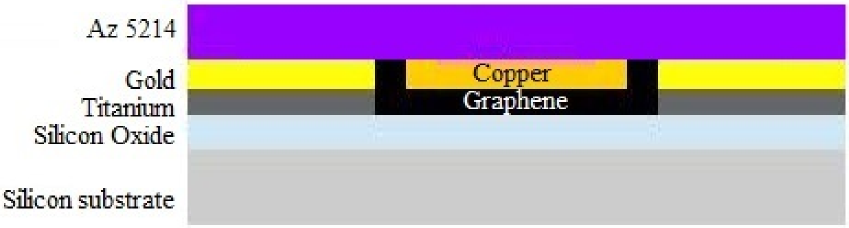

Figure 7.8: Electrolite gated GFET: Az 5214 layer deposition and photo lithographic step

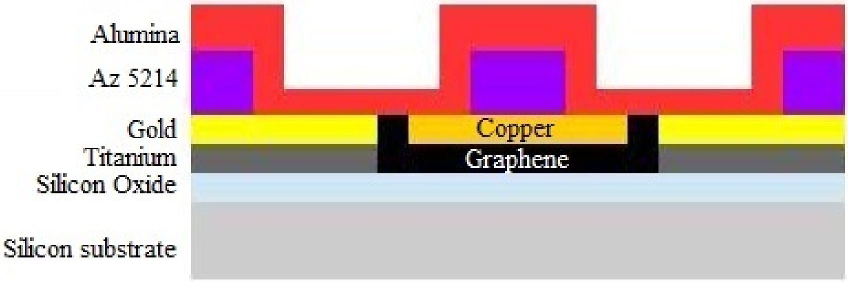

Figure 7.9: Electrolite gated GFET: Alumina EBPVD

The Alumina is lifted off from the areas covered by the Az 5214 photoresist, leaving exposed the Gold contact pads and the channel (fig. 7.10). The last operation, in order to complete the electrolyte gated GFET process flow, is to etch the Copper in a Ferric chloride bath, exposing definitively the graphene channel.

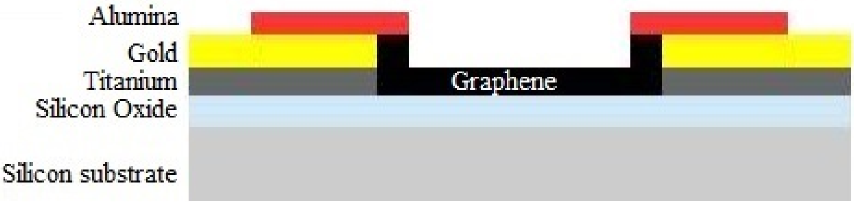

Figure 7.10: Electrolite gated GFET: Alumina lift off and Copper etching

At the end of the process flow, the chip housing the array of ten transistor is ready to be electrically characterized (fig. 7.11). According with the design, it is possible to modify the channel dimension of each transistor in order to acquire different electrical measurement and acquire multiple data with a sigle chip design.

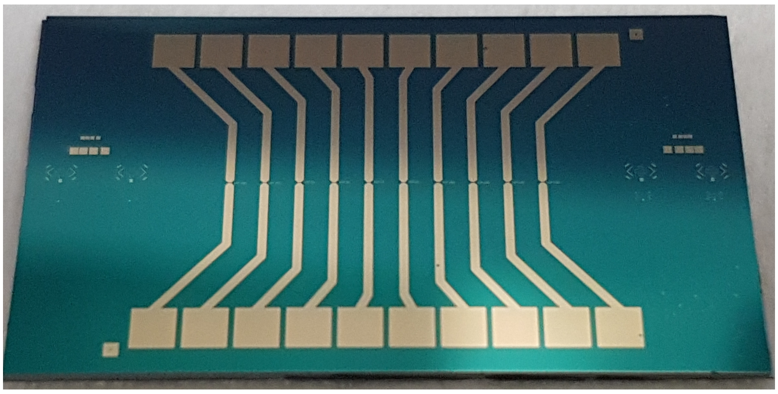

Figure 7.11: Electrolite gated GFET: completed chip

7.2 Electrolyte gated GFET - Electrical response

GFET demonstrates ambipolar curve under the electric field effect. Its conductivity is driven by charge carriers (hole and electrons) in graphene channel. As gate voltage increases, the conductivity of GFET increases with the increasing concentration of electrons (or holes) induced by positive (or negative) gate voltages. The changes in carrier concentration of graphene channel are controlled by Fermi level of graphene which is continuously driven from conduction (or valence) band to valence (or conduction) band via Dirac point as gate voltage is applied. Under negative gate bias, Fermi level drops below Dirac point to introduce significant amount of holes in valance band, while under positive gate bias Fermi level rise above Dirac point to introduce reliable amount of electrons into conduction band.
The graph of drain current I_d versus gate voltage V_G represents the transfer characteristics of GFET. Looking at the graph, I_d is a function of the gate voltage, V_d is the drain voltage that sweep from 0.1V to 0.4V by step of 0.1V. This transfer characteristics curve illustrates that the conduction of GFET exhibits ambipolar characteristics. The minimum conductivity of GFET occurs at $V_G = 1V$ which defines the Dirac point ,or charge neutrality point, of the curve. This shows that GFET experienced highest resistivity and minimum conductivity at this point.
As V_d increase, the Dirac point shift towards higher values indicating that the drain voltage had direct influence on the channel potential, the magnitude of drain current also increase with increasing V_d (fig. 7.12). This shows also that external factors such as doping or graphene functionalization can influence the surface charges of the GFET. [20]

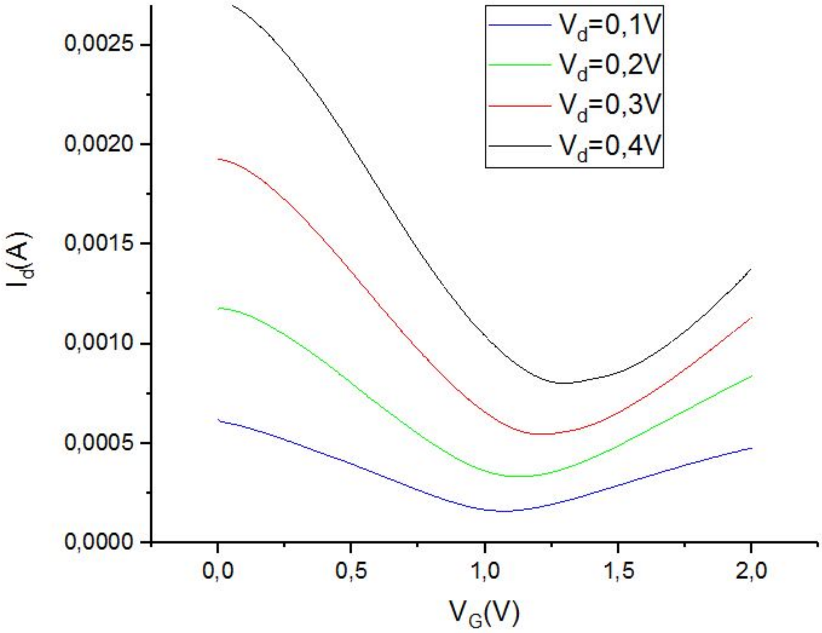

Figure 7.12: Electrolyte gated GFET Transfer characteristic, transfer mediated by PMMA supporting layer

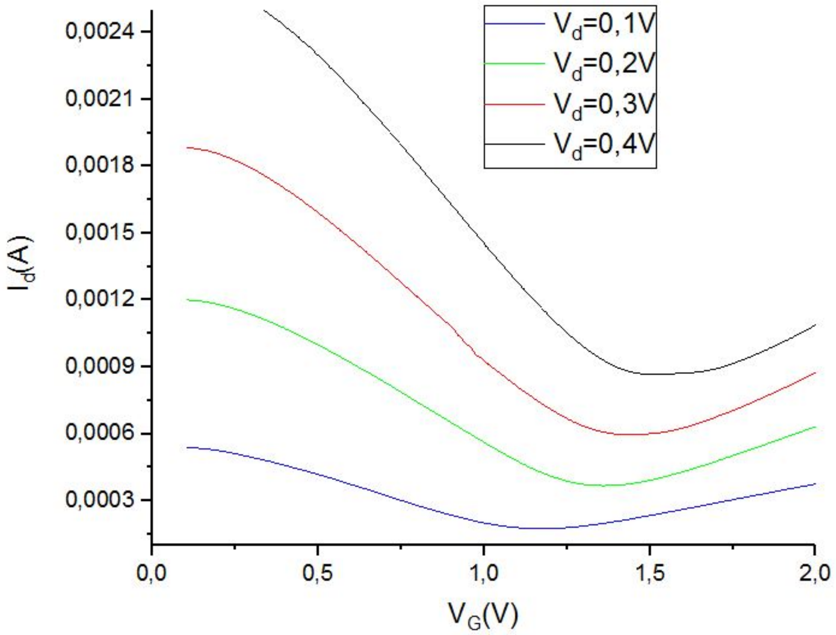

Figure 7.13: Electrolyte gated GFET Transfer characteristic, Transfer mediated by Shellac supporting layer

As it is possible to deduce from the graphs (fig. 7.12 - 7.13), the graphene electrical properties are not influenced by the kind of supportive layer chosen for assisting the transfer process. The Dirac point on both the graphs occurs at a lightly higher V_G than the expected $0V$, this behavior could depend on an intrinsic defectiveness of the graphene channel or it could depend on a defective realization of the transistor array.

Chapter 8

Conclusions

Through the identification of the best graphene growth and transfer recipes, optimized to the production of a low defective and monolayer graphene, it is possible to build up the channel component of an Electrolyte Gated Graphene Field Effect Transistor (ref. paragraph 3.39). The GFET has been used to test and practically characterize, from an electrical point of view, the properties of the graphene monolayer .

As shown in chapter 6, the Chemical Vapor Deposition is a process that allow to obtain a low cost and high quality graphene (fig. 2.5). Looking at the Raman spectra obtained from the best quality sample (ref. paragraph 5.1 and fig 6.7), it is possible to notice the high ratio (more than 3 times) between the intensities of the 2D-peak and the G-peak which proof his monolayer constitution (ref. paragraph 6.0.1). Moreover, studying shape and intensity of the G-peak (fig. 6.10), which is strongly correlated with the defectiveness of the monolayer, it is possible to notice that its shape, which is narrow and short, highlights its low quantity of defects.

The transfer process (ref paragraph 5.2), which can be performed using PMMA or Shellac solutions as supporting layer, is absolutely mandatory in order to remove the Copper layer (only necessary in the growth stage) and transfer the graphene layer onto the desired substrate. It is fundamental to understand that the transfer process does not influence the monolayer characteristic of graphene, since it only depend on the growth stage. However it is important to remind that an incorrect transfer process will induce an high quantity of defects in the graphene (like cracks and wrinkles which are visible by the shape of the G-peak spectra, ref. paragraph 6.0.1, fig. 6.10a), and it may decrease the efficiency of its electrical and physical properties.

In order to test the electrical response of the graphene monolayer, it has been used in an Electrolyte Gated Graphene Field Effect Transistor as conductive channel. As shown in chapter 7, the electrical response is coherent with the graphene monolayer behavior (fig. 7.12 - 7.13), demonstrating an ambipolar trans characteristic curve under the electric field effect. This particular response, which is coherent between both the graphene samples transfered with PMMA and Shellac, highlights that the two transfer procedures are equivalent from an electrical point of view, and so is the quality of the transferred graphene.

Chapter 9

Appendix

9.1 Riassunto

Nell'elaborato sono state descritte tutte le procedure che, durante il percorso di tesi, hanno portato alla produzione di grafene monolayer ed alla realizzazione di un transistor di tipo "Electrolyte Gated Graphene Field Effect Transistor". Il quale è stato costruito con lo scopo di caratterizzare, da un punto di vista puramente elettrico, il grafene prodotto.
Nel capitolo 2 viene descritto il grafene: inizialmente nella sua struttura fisica per poi passare alle proprietà meccaniche, le quali lo attestano come uno dei materiali più resistenti attualmente conosciuti. Sono poi stati descritti nel dettaglio i più comuni ed efficaci processi di produzione del grafene, prestando particolare attenzione ai confronti fra di essi. Si evince pertanto che il miglior metodo di produzione massiva del grafene, per qualità del risultato e contenimento dei costi, risulta essere la Chemical Vapor Deposition (CVD).
Nel capitolo 3 vengono descritte ed argomentate le caratteristiche di un "Field Effect Transistor", di cui sono spiegati i principi che ne determinano il funzionamento e le principali conseguenze della riduzione delle sue dimensioni fisiche. L'impiego del grafene come canale in un sistema FET aiuta a ridurre notevolmente i difetti (Short Channel Effects) dovuti alla miniaturizzazione del sistema, mantenendone pressochè invariati i vantaggi. E' fondamentale evidenziare che, data la particolare struttura fisica del grafene, esso renderà molto difficile l'ottenimento di una condizione di completo spegnimento del transistor, rendendo di fatto il suo impiego molto selettivo in base alla destinazione d'uso.
Nel capitolo 4 vengono esaminate le tecnologie che sono state utilizzate per produrre e caratterizzare i campioni di grafene studiati durante il percorso di tesi. Viene descritto interamente il sistema di Chemical Vapor Deposition da banco *Moorefield nanotechnology nanoCVD-8G* (utilizzato per la produzione dei campioni di grafene), evidenziando nel dettaglio la struttura fisica e le modalità di funzionamento. Successivamente viene presentato il sistema di Eectron-beam Physical Vapor Deposition *ULVAC*, il quale è stato utilizzato nei processi di produzione dell' Electrolyte Gated GFET unitamente al Mask Aligner. Di entrambe le tecnologie vengono

descritti i principi di funzionamento e la struttura.
La principale tecnologia per la caratterizzazione dei campioni di grafene prodotti in laboratorio risulta essere la Spettroscopia Raman, la quale è fondamentale per identificare se il campione di grafene è monolayer e la quantità di difetti (come cricche o rugosità) presenti sulla sua superficie. A questa caratterizzazione sono state affiancate altre tecnologie come il Field Emission Scanning Electron Microscopy (FESEM), utile per ispezionare la superficie del campione di grafene, allo scopo di indagare riguardo la presenza di grandi residui del processo di lavorazione. Unitamente all' X-Ray Photolectron Spectroscopy (XPS) rivelatosi fondamentale per identificare eventuali residui di elementi estranei al processo produttivo o eventuali contaminazioni.
Nel capitolo 5 viene descritta la tecnica di crescita dei campioni di grafene prodotti in laboratorio. La quale prevede l'utilizzo di un substrato "in foglia" di Rame che, dopo un processo di rimozione dell'ossido naturamente presente sulla sua superficie, catalizzerà la crescita di un monolayer di grafene. La ricetta ottimizzata per la produzione di grafene mediante Chemical Vapor Deposition è quindi completamente esplicitata nel dettaglio. Il processo di trasferimento del grafene dal substrato di Rame, il quale deve essere rimosso, al substrato di destinzione (Silicio nel caso dei campioni prodotti in laboratorio), viene effettuato mediante il sostegno meccanico di un polimero che deve presentare al contempo caratteristiche di resistenza ed elasticità. Sono perciò stati testati due polimeri: PMMA (in soluzione di anisolo) e Gommalacca (in soluzione di etanolo), i quali hanno prodotto risultati positivi per il trasferimento.
Nel capitolo 6 vengono presentate tutte le caratterizzazioni, effettuate mediante le tecnologie precedentemente descritte, che dimostrano l'efficacia della ricetta di produzione del grafene tramite Chemical Vapor Deposition, e la buon qualità dei trasferimenti mediati da entrambi i polimeri.
Nel capitolo 7 viene esplicitato tutto il processo di produzione di un Electrolyte Gated GFET, il quale viene utilizzato per caratterizzare elettricamente il grafene prodotto e trasferito secondo le tecniche precedentemente illustrate. Il transistor presenta una caratteristica ambipolarità, facilmente identificabile nei grafici proposti e tipica della presenza di un canale in grafene. Questo comportamento è un ulteriore indice della buona qualità del grfene prodotto e trasferito.

9.2 Summary

This thesis aims to describe all the procedures that allows the production of monolayer graphene and the realization of an "Electrolyte Gated Field Effect Transistor". This device was built in order characterize the graphene from an electrical point of view.

The chapter 2 describes the graphene: its physic structure and mechanical properties, which qualify it as one of the most resistant materials nowadays known.

The most common graphene production processes are then described and compared.

The chapter 3 describes the Field Effect Transistor characteristics, explaining its functioning principles and the consequences of its physical shrinking. The use of graphene as conductive channel helps to highly reduce the "Short Channel Effects", maintaining almost intact the benefits of a dimension reduction. Is important to highlight that, due to its particular physics structure and electrical properties, graphene as conductive channel will prevent the achievement of a complete transistor shutdown. This peculiarity makes graphene transistor suitable only in particular intended use.

The chapter 4 describes the technology used in order to produce and characterize the graphene samples studied during the thesis. Particular attention is dedicated to the Chemical Vapor Deposition bench machine *Moorefield nanotechnology nonoCVD-8G* (used for the graphene sample production), highlighting in details its physical structure and operating modes. Subsequently is presented the Electron Beam Physical Vapor Deposition machine *ULVAC*, used in the production processes of the Electrolyte Gated GFET together with the mask aligner machine, of both technologies the operation modes and the structure are explained.

The major technology used to characterize graphene samples is the Raman Spectroscopy, which is fundamental in order to identify the sample as monolayer or multilayer and in order to estimate the quantity of defects laying on its surface.

This characterization has been joined by others such as Field Emission Scanning Microscopy (FESEM), useful to inspect the graphene sample surface searching processing residues, and X-Ray Photoelectron Spectroscopy (XPS), useful to identify contamination by elements unrelated to the process.

The chapter 5 describes the graphene growth technique used in the laboratory process. After an oxide removal process, a copper thin foil will catalyze the growth of a graphene monolayer in a CVD chamber environment. The optimized monolayer graphene production recipe is explained in detail.

The graphene transfer process, from the old copper substrate to the new silicon substrate is made though the mechanical supportive action of a polymer. PMMA (in Anisole solution) and Shellac (in ethanol solution) have both produced positive results.

The chapter 6 describes the production process of an Electrolyte Gated GFET, which has been used to characterize the graphene samples from an electrical point of view. The transistor shows a characteristic ambipolarity, typical of the presence of a graphene conductive channel. This behavior is a further confirmation of the good quality of the produced graphene.

Bibliography

[1] H. Zhu, Z. Xu, D. Xie, and Y. Fang, *Graphene : fabrication, characterizations, properties and applications.* Elsevier, 2017.

[2] D. G. Papageorgiou, I. A. Kinloch, and R. J. Young, "Mechanical properties of graphene and graphene-based nanocomposites," *Progress in Materials Science*, vol. 90, pp. 75–127, 2017.

[3] J. Angela and S. Nathaniel, "Mechanical Exfoliation to Make Graphene," tech. rep., University of Wisconsin – Madison, 2004.

[4] X. Chen, L. Zhang, and S. Chen, "Large area CVD growth of graphene," *Synthetic Metals*, vol. 210, pp. 95–108, dec 2015.

[5] A. Kumar and C. Huei, "Synthesis and Biomedical Applications of Graphene: Present and Future Trends," in *Advances in Graphene Science*, InTech, jul 2013.

[6] A. Matković, I. Milošević, M. Milićević, T. Tomašević-Ilić, J. Pešić, M. Musić, M. Spasenović, D. Jovanović, B. Vasić, C. Deeks, R. Panajotović, M. R. Belić, and R. Gajić, "Enhanced sheet conductivity of Langmuir-Blodgett assembled graphene thin films by chemical doping," *2D Materials*, vol. 3, p. 015002, jan 2016.

[7] P. Yu, S. E. Lowe, G. P. Simon, and Y. L. Zhong, "Electrochemical exfoliation of graphite and production of functional graphene," *Current Opinion in Colloid and Interface Science*, vol. 20, pp. 329–338, oct 2015.

[8] C. P. P. Wong, C. W. Lai, K. M. Lee, and S. B. Abd Hamid, "Advanced chemical reduction of reduced graphene oxide and its photocatalytic activity in degrading reactive black 5," *Materials*, vol. 8, pp. 7118–7128, oct 2015.

[9] D. Reddy, L. F. Register, G. D. Carpenter, and S. K. Banerjee, "Graphene field-effect transistors," *Journal of Physics D: Applied Physics*, vol. 45, no. 1, p. 019501, 2012.

[10] F. Schwierz, "Graphene transistors," *Nature Nanotechnology*, vol. 5, pp. 487–496, jul 2010.

[11] S. Liu and X. Guo, "Carbon nanomaterials field-effect-transistor-based biosensors," *NPG Asia Materials*, vol. 4, pp. e23–e23, aug 2012.

[12] C. E. Mackin, *Electrolyte-Gated Graphene Field-Effect Transistors: Modeling and Applications*. PhD thesis, Massachusetts Institute of Technology, 2015.

[13] Y. Y. Wang, Z. H. Ni, T. Yu, Z. X. Shen, H. M. Wang, Y. H. Wu, W. Chen, and A. T. S. Wee, "Raman studies of monolayer graphene: The substrate effect," *Journal of Physical Chemistry C*, vol. 112, no. 29, pp. 10637–10640, 2008.

[14] A. C. Ferrari, "Raman spectroscopy of graphene and graphite: Disorder, electron-phonon coupling, doping and nonadiabatic effects," *Solid State Communications*, vol. 143, no. 1-2, pp. 47–57, 2007.

[15] A. C. Ferrari and D. M. Basko, "Raman spectroscopy as a versatile tool for studying the properties of graphene," *Nature Nanotechnology*, vol. 8, no. 4, pp. 235–246, 2013.

[16] A. Y. Zhu, F. Yi, J. C. Reed, H. Zhu, and E. Cubukcu, "Optoelectromechanical multimodal biosensor with graphene active region," *Nano Letters*, vol. 14, no. 10, pp. 5641–5649, 2014.

[17] G. B. Barin, Y. Song, I. D. F. Gimenez, A. G. S. Filho, L. S. Barreto, and J. Kong, "Optimized graphene transfer: Influence of polymethylmethacrylate (PMMA) layer concentration and baking time on grapheme final performance," *Carbon*, vol. 84, no. C, pp. 82–90, 2015.

[18] I. Platzman, R. Brener, H. Haick, and R. Tannenbaum, "Oxidation of polycrystalline copper thin films at ambient conditions," *Journal of Physical Chemistry C*, vol. 112, pp. 1101–1108, jan 2008.

[19] D. S. Choi, K. S. Kim, H. Kim, Y. Kim, T. Y. Kim, S. H. Rhy, C. M. Yang, D. H. Yoon, and W. S. Yang, "Effect of cooling condition on chemical vapor deposition synthesis of graphene on copper catalyst," *ACS Applied Materials and Interfaces*, vol. 6, pp. 19574–19578, nov 2014.

[20] R. S. Selvarajan, A. A. Hamzah, and B. Y. Majlis, "Transfer Characteristics of Graphene based Field Effect Transistor (GFET) for Biosensing Application," in *2017 IEEE Regional Symposium on Micro and Nanoelectronics (RSM)*, pp. 88–91, 2017.